Article

Current Biology

Coinfecting phages impede each other's entry into the cell

Graphical abstract

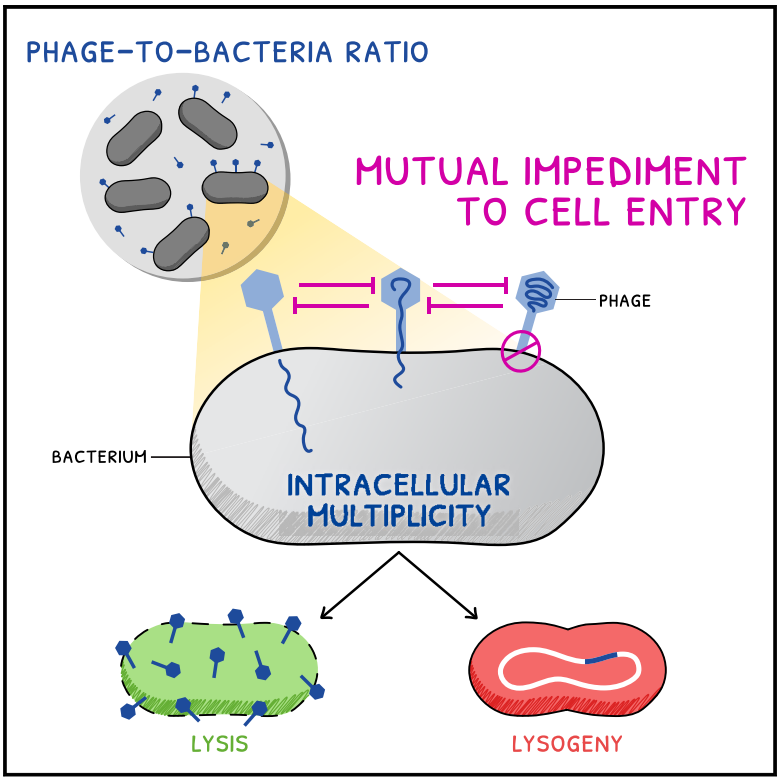

Authors

Thu Vu Phuc Nguyen, Yuchen Wu, Tianyou Yao, Jimmy T. Trinh, Lanying Zeng, Yann R. Chemla, Ido Golding

Correspondence

igolding@illinois.edu

In brief

Nguyen et al. find that when multiple lambda phages infect the same *E. coli* cell, they slow or even prevent each other from entering the cell. Similar behavior is observed in other phages. The impeded entry at high multiplicities, caused by phage-induced perturbation to the host cell, impacts the choice between viral reproduction and dormancy.

Highlights

- Adsorption and genome entry of individual phages were followed in real time
- The efficiency of phage entry decreases at higher multiplicity of infection (MOI)
- Phage entry is impeded at high MOI by adsorption-induced perturbation to the cell
- MOI-dependent phage entry impacts the choice between lysis and lysogeny

Nguyen et al., 2024, Current Biology *34*, 1–13
July 8, 2024
https://doi.org/10.1016/j.cub.2024.05.032

CellPress

Please cite this article in press as: Nguyen et al., Coinfecting phages impede each other's entry into the cell, Current Biology (2024), https://doi.org/10.1016/j.cub.2024.05.032

Current Biology

CellPress

Article

Coinfecting phages impede each other's entry into the cell

Thu Vu Phuc Nguyen,[1,2,7] Yuchen Wu,[3] Tianyou Yao,[1] Jimmy T. Trinh,[4,5] Lanying Zeng,[4,5] Yann R. Chemla,[1,3] and Ido Golding[1,2,6,8,*]

[1]Department of Physics, University of Illinois Urbana-Champaign, Urbana, IL 61801, USA
[2]Verna and Marrs McLean Department of Biochemistry and Molecular Biology, Baylor College of Medicine, Houston, TX 77030, USA
[3]Center for Biophysics and Quantitative Biology, University of Illinois Urbana-Champaign, Urbana, IL 61801, USA
[4]Department of Biochemistry and Biophysics, Texas A&M University, College Station, TX 77843, USA
[5]Center for Phage Technology, Texas A&M University, College Station, TX 77843, USA
[6]Department of Microbiology, University of Illinois Urbana-Champaign, Urbana, IL 61801, USA
[7]Present address: Department of Molecular Biology, Princeton University, Princeton, NJ 08544, USA
[8]Lead contact
*Correspondence: igolding@illinois.edu
https://doi.org/10.1016/j.cub.2024.05.032

SUMMARY

The developmental choice made by temperate phages, between cell death (lysis) and viral dormancy (lysogeny), is influenced by the relative abundance of viruses and hosts in the environment. The paradigm for this abundance-driven decision is phage lambda of *E. coli*, whose propensity to lysogenize increases with the number of viruses coinfecting the same bacterium. It is believed that lambda uses this number to infer whether phages or bacteria outnumber each other. However, this interpretation is premised on an accurate mapping between the extracellular phage-to-bacteria ratio and the intracellular multiplicity of infection (MOI). Here, we show this premise to be faulty. By simultaneously labeling phage capsids and genomes, we find that, while the number of phages landing on each cell reliably samples the population ratio, the number of phages entering the cell does not. Single-cell infections, performed in a microfluidic device and interpreted using a stochastic model, reveal that the probability and rate of phage entry decrease with the number of adsorbed phages. This decrease reflects an MOI-dependent perturbation to host physiology caused by phage attachment, as evidenced by compromised membrane integrity and loss of membrane potential. The dependence of entry dynamics on the surrounding medium results in a strong impact on the infection outcome, while the protracted entry of coinfecting phages increases the heterogeneity in infection outcome at a given MOI. Our findings in lambda, and similar results we obtained for phages T5 and P1, demonstrate the previously unappreciated role played by entry dynamics in determining the outcome of bacteriophage infection.

INTRODUCTION

Bacteriophage lambda serves as a paradigm for the decision made by temperate phages between rampant replication, resulting in the release of viral progeny and cell death (lysis) and dormancy in a prophage state (lysogeny), which allows the host bacterium to live and reproduce.[1,2] The best-characterized factor affecting this choice is the number of lambda phages coinfecting the cell (multiplicity of infection [MOI]).[3,4] Infection by a single phage typically results in lysis, whereas a higher MOI results in lysogeny.[5,6] The effect of MOI is mediated by a phage-encoded circuit that chooses the transcriptional program to be executed based on the number of lambda genomes that entered the cell.[7,8] In terms of its utility, viral self-counting is believed to serve as a way of inferring the abundance of available hosts in the environment.[3,9] Specifically, simultaneous infection by multiple phages (i.e., MOI > 1) implies that phages outnumber bacteria, thus the release of new progeny via lysis will be futile, and lysogeny should be chosen. This interpretation is consistent with other examples where the relative abundance of phages and bacteria impacts infection outcome.[10] However, it is premised on an accurate mapping between the environmental phage-to-bacteria ratio and the intracellular MOI, a mapping that has not been directly tested. This accurate mapping is further called into doubt by the fact that, at the single-cell level, the relation between MOI and infection outcome is highly probabilistic rather than threshold-like.[6,11] Thus, the relationship between the population ratio and the number of internalized phage genomes merits careful examination.

Another motivation to closely inspect phage entry is that our understanding of the process remains fragmentary, even for a system as extensively studied as lambda.[2] For one, there is no consensus regarding the nature of physical forces driving translocation of the encapsidated DNA into the cell.[12] Several competing hypotheses exist, including DNA self-repulsion followed by diffusion,[13] and hydrodynamic drag due to water drainage through the capsid,[14] but the available data are insufficient to determine their veracity. Also unclear is the exact route

Please cite this article in press as: Nguyen et al., Coinfecting phages impede each other's entry into the cell, Current Biology (2024), https://doi.org/10.1016/j.cub.2024.05.032

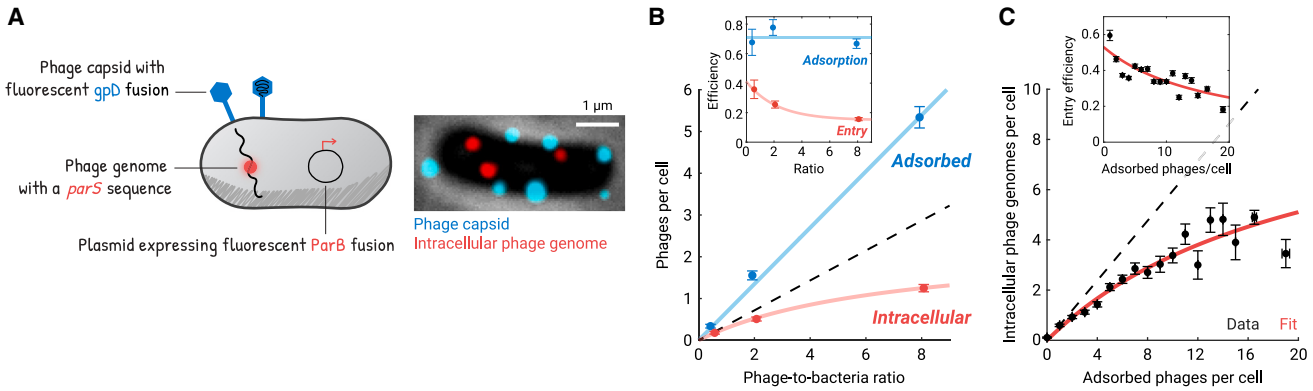

Figure 1. The intracellular viral copy number is not proportional to the extracellular phage-to-bacteria ratio

(A) Phage capsids and intracellular phage genomes were fluorescently labeled. Left: schematic of the labeling system. Right: an *E. coli* cell adsorbed by seven lambda phages (cyan spots), three of which have ejected their genomes (red spots). The infection mixture was imaged 5 min after triggering genome ejection. The image shown is a maximum projection of multiple focal planes, spanning the height of the cell.

(B) The fraction of phages whose genomes entered the cell decreases at higher phage-to-bacteria ratio. Phages and bacteria were mixed at different ratios. Markers, mean ± SE for the average numbers of adsorbed and intracellular phages (n = 201, 204, and 221 cells for samples with mixing ratios of 0.5, 2, and 8, respectively). Cyan line, linear fit. Red curve, fit to a Michaelis-Menten function, serving as a guide to the eye. Dashed line, linear scaling extrapolated from the sample with the phage-to-bacteria ratio of 0.5. Inset: the efficiencies of phage adsorption and entry (defined as the average numbers of adsorbed and intracellular phages per cell, respectively, divided by the phage-to-bacteria ratio).

(C) The number of intracellular phage genomes scales sublinearly with the number of phages adsorbed to the cell. Black markers, mean ± SE (n = 1,437 cells, pooled from 7 independent experiments); cells at higher MOI were binned together to allow for at least 10 cells per bin. Red curve, fit to a Michaelis-Menten function, serving as a guide to the eye. Dashed line, linear scaling extrapolated from cells with one adsorbed phage. Inset: the efficiency of phage entry as a function of the number of adsorbed phages. The red curve was calculated using the same fit as in the main panel.

See also Figure S1.

the phage genome takes to enter the cell: the maltoporin LamB (lambda receptor) is involved in the initial reversible binding to the host surface,[15] the eventual irreversible docking at the site where DNA will cross the cell membrane,[16] and in triggering DNA entry.[17] It is unlikely, however, that phage DNA moves *through* the LamB porin.[18,19] Instead, it is suggested that the phage's tape measure protein (gpH) breaches the outer membrane and then acts as a conduit for DNA translocation through the bacterial periplasm.[19–22] Similarly elusive is how lambda DNA crosses *E. coli*'s inner membrane. Whereas penetration generally requires the inner-membrane mannose phosphotransferase system (PtsM or Man-PTS),[23,24] phages with extended genomes and those harboring certain tail mutations can overcome this requirement.[21,25] Thus, how lambda DNA and PtsM interact during phage entry also remains an open question. Critically, our picture of phage entry is largely inferred from studies of isolated components *in vitro* and from bulk studies where single-cell kinetics remains hidden.[12] There is thus considerable benefit to examining the entry process in its true context of infection, at the resolution of individual phages and cells.

RESULTS

The intracellular viral copy number is not proportional to the extracellular phage-to-bacteria ratio

To examine infection at the single-cell level, we utilized phages (λ *cI857 Pam80 stf*::P1*parS-kan*^{R})[8] whose capsid was decorated with gpD-mTurquoise2 or gpD-EYFP.[26] Following infection (of host MG1655), the intracellular phage genome is detected via binding of mCherry-ParB or CFP-ParB to an engineered *parS* sequence[27,28] (Figure 1A; STAR Methods). The infecting phage is unable to replicate on wild-type host, preventing intracellular genome number from increasing after entry.[8] The labeling scheme enables reliable counting of both extracellular capsids and intracellular phage genomes (Figure S1).

We first asked how the numbers of phages adsorbed (irreversibly attached[29,30]) to the cell and of phages that have entered the cell (intracellular genomes) changed as we infected cells with varying phage concentrations. Cells grown in LB (supplemented with maltose and $MgSO_4$) were concentrated, mixed with phages, and incubated at 4°C for 30 min to allow adsorption; then, to trigger genome ejection, the infection mixture was shifted to 35°C[6,8,29] (STAR Methods). Imaging the infected samples at 5 min after triggering, we found that, over an ~10-fold change in phage concentration, the average number of adsorbed phages per cell followed the phage-to-bacteria ratio (Figure 1B), with the adsorption efficiency remaining constant at 0.71 ± 0.04 (mean ± SE of three samples, n = 201, 204, and 221 cells), consistent with reported values[31–33] (Figure S1). By contrast, the efficiency of phage entry decreased approximately 2-fold (from 0.36 ± 0.06 to 0.16 ± 0.01; Figure 1B). Consequently, the average number of intracellular phage genomes per cell did not reflect the bulk ratio of phages to bacteria.

We next utilized the natural variability in the number of phages adsorbed to each cell[6,8] to probe the relation between the adsorbed and intracellular phage numbers at the single-cell level. We found that as the number of adsorbed phages per cell increased, the efficiency of phage entry decreased: from approximately 60% in cells adsorbed by a single phage (consistent with previous reports[29,33]; Figure S1) to approximately 30% in cells adsorbed by 10 phages (Figure 1C; n = 1,437 cells, pooled from 7 independent experiments). As a result, the number

Please cite this article in press as: Nguyen et al., Coinfecting phages impede each other's entry into the cell, Current Biology (2024), https://doi.org/10.1016/j.cub.2024.05.032

CellPress

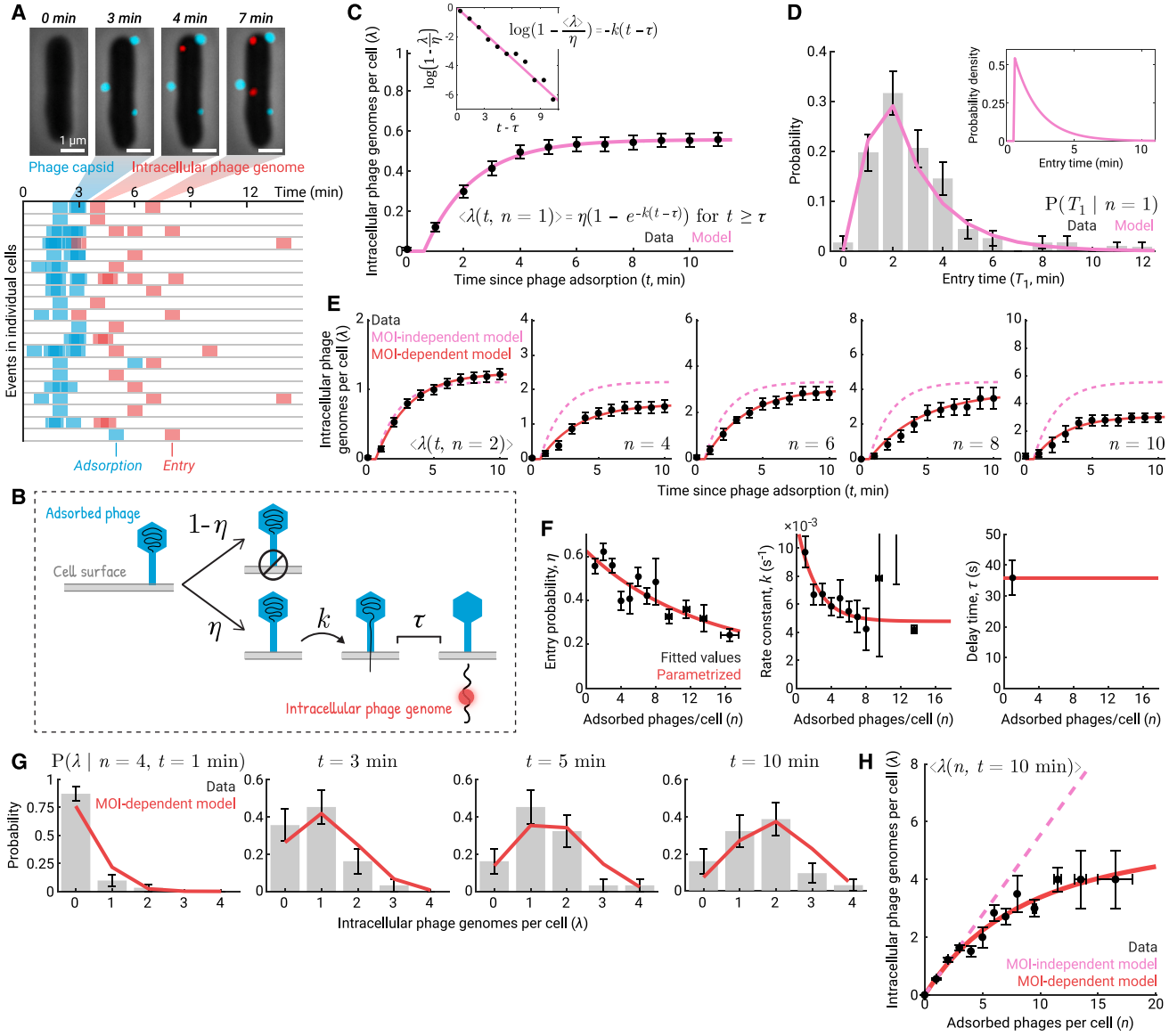

Figure 2. Time-lapse measurements indicate an MOI-dependent decrease in the probability and rate of phage entries

(A) Adsorption and entry of individual phages were followed in a microfluidic device. Top: an infected cell tracked over time. Bottom: for each cell, the times of adsorption and entry events were recorded. Data for 20 cells are shown. For all cells in this experiment, see Figure S2.

(B) Schematic of the stochastic model for phage entry kinetics; see text for details.

(C) The theoretical model captures the time-dependent average number of intracellular phages in cells adsorbed by one phage. Black markers, mean ± SE (n = 208 cells, pooled from 7 independent experiments). Pink curve, fit to the model. Inset: linearized data and model.

(D) The model successfully predicts the distribution of entry times in cells adsorbed by one phage. Gray bars, histogram of the data, with error bars indicating SE. Pink curve, the probability distribution predicted by the model, binned by the imaging inter-frame interval. Inset: the theoretical probability distribution before binning.

(E) A dependence of the entry parameters on the number of adsorbed phages is required to capture the experimental data. Dashed curves in pink, predictions by a model in which η and k in cells adsorbed by multiple phages are equal to those in cells adsorbed by a single phage. Solid curves in red, predictions by a model in which η and k are allowed to vary with the number of adsorbed phages. Black markers, data ± SE for cells adsorbed by 2, 4, 6, 8, and 10 phages. For other MOIs, see Figure S2.

(F) Inferred parameters for the MOI-dependent model. Black markers, fitted values ± SE from bootstrapping (n = 1,030 cells, pooled from 7 independent experiments); cells at higher MOI were binned together to allow for at least 10 cells per bin. Red curves, parametrization: η and k as exponentially decaying functions of the number of adsorbed phages, τ remaining the same as in cells adsorbed by a single phage.

(G) The MOI-dependent model successfully predicts the distributions of intracellular phage numbers at a given time. Gray bars, histograms of the data, with error bars indicating SE. Red curves, model predictions. Data for cells adsorbed by 4 phages at 1, 3, 5, and 10 min are shown. For other MOIs and other time points, see Figure S2.

(legend continued on next page)

Please cite this article in press as: Nguyen et al., Coinfecting phages impede each other's entry into the cell, Current Biology (2024), https://doi.org/10.1016/j.cub.2024.05.032

of intracellular phage genomes scales sublinearly with the number of adsorbed phages (Figure 1C). To exclude the possibility that this reduced efficiency is an artifact of our capsid or genome labeling schemes, we used SYTOX orange (a DNA-intercalating dye) to visualize DNA ejection[34,35] from non-fluorescent capsids into cells that did not express fluorescent ParB fusions (Figure S1; STAR Methods). We again found that, as more phages adsorbed to the cell, the efficiency of phage ejection decreased (Figure S1). Altogether, our results thus indicate that lambda entry becomes impeded at high multiplicities of infection.

Time-lapse measurements indicate an MOI-dependent decrease in the probability and rate of phage entries

To gain insight into the observed reduction in entry efficiency, we next aimed to examine the temporal kinetics of phage entries in individual cells. To that end, we performed infection in a microfluidic device, tracking phage adsorption and entry in real time (Figure 2A; STAR Methods). The experiments provided the time series of phage adsorption and entry events in each infected cell (Figure 2A; see Figure S2 for additional cells). To interpret these time series and identify which aspect of viral entry is perturbed at high multiplicities, we formulated a simple stochastic model where phage entry is governed by three parameters (Figure 2B): η, the entry probability (at infinite time); k, the rate (or probability per unit time) of initiating entry; and τ, the time between entry initiation and detection (STAR Methods for the full model description). For a cell adsorbed by n phages, the model is solved to yield the probability distribution for the number of intracellular phage copies at time t. We first tested the model on cells adsorbed by a single phage ($n = 1$). The model successfully captured the time-dependent average number of intracellular phages $\langle\lambda(t, n = 1)\rangle$ (Figure 2C) and the distribution of phage entry time $P(T_1|n = 1)$ (Figure 2D). The inferred parameter values ($\eta = 0.56 \pm 0.04$, $1/k = 1.7 \pm 0.2$ min, $\tau = 35.9 \pm 5.6$ s, $n = 208$ cells pooled from 7 independent experiments, SE from bootstrapping) were consistent with the entry efficiency and mean entry time we observed in bulk and with reported values[26,29,33,34,36] (Figure S1), thus lending credence to the microfluidic-acquired data and the stochastic model used to interpret it.

Having calibrated our model based on singly infected cells, we aimed to use it to predict the entry kinetics in cells adsorbed by two or more phages (Figure 2E). We first tested the null hypothesis that the parameters inferred from cells adsorbed by one phage also govern the kinetics in cells adsorbed by multiple phages ("MOI-independent model"). We found, however, that as the number of adsorbed phages increased, the prediction of intracellular phage number became poorer. In particular, the MOI-independent model overestimated the average number of intracellular phages at any given time (Figures 2E and S2). This was no surprise, considering our observations above (Figure 1C), which indicated a decrease in phages' ability to enter the cell at higher multiplicities. Aiming to capture that effect, we allowed model parameters to now vary with the number of adsorbed phages ("MOI-dependent model"). The revised model successfully reproduced the average kinetics (Figure 2E) and revealed a decrease in both entry probability η and rate k with the number of adsorbed phages per cell (Figure 2F); no MOI dependence of τ was required to capture the data (see Figure S2 for all model variations). Parametrizing η and k as exponentially decaying functions of the number of adsorbed phages, the stochastic model also captured the distributions of intracellular phage numbers at a given time (Figures 2G and S2). Finally, the model successfully reproduced the sublinear relation between the numbers of intracellular and adsorbed phages observed in both the microfluidic and bulk experiments (Figures 2H and S2). The time-lapse analysis of infection thus indicates an MOI-dependent decrease in the probability and rate of phage entries.

Phage adsorption causes cellular perturbation, resulting in impeded phage entry

How does coinfection impede phage entry into the cell? As mentioned above, the successful ejection of lambda DNA into the cell requires both LamB and PtsM.[2,19] It is conceivable that, in cells adsorbed by multiple phages, one or both of these factors become the limited resource for entry. To test this hypothesis, we performed infections of cells grown in media supplemented by either maltose or glucose (STAR Methods). The latter sugar is known to repress the expression of both LamB and PtsM,[37,38] as well as the activity of PtsM.[39] Consistent with previous reports,[37] we found that maltose-grown cells exhibited higher efficiency of lambda adsorption (Figure S3). However, no difference in entry efficiency was seen between maltose and glucose, and the same sublinear relation between the numbers of adsorbed and intracellular phages was observed in both cases (Figure S3). Our data thus suggest that LamB or PtsM levels do not drive the impedance to entry at high multiplicities.

We next asked whether the impeded entry reflects the activity of an unidentified factor produced upon early phage entries by either those phages themselves (acting as an exclusion factor[40]) or, in response to entry, by the host (as part of an anti-phage defense mechanism[41]). To test this idea, we performed infection in the presence of rifampicin, an inhibitor of transcription[42] (STAR Methods). As expected, we found that both cell growth and viral development were strongly repressed in the presence of the drug (Figure S3). However, lambda entry was not significantly impacted and exhibited the familiar reduction in efficiency as the number of adsorbed phages increased (Figure S3). We therefore concluded that impeded entry is not mediated by a factor expressed by either phage or host upon the initial viral entry.

In searching for an alternative explanation for the MOI-dependent impediment to phage entry, we revisited several reported aspects of early infection. First, phage infection induces a strong ionic perturbation to the host cell, involving fluxes of solutes and a reduction or even loss of membrane potential.[43,44] Phage-induced perturbations were reported for diverse phage and bacterial species, including lambda and *E. coli*.[43,45,46] The severity of

(H) The MOI-dependent model reproduces the sublinear relation between the numbers of adsorbed and intracellular phages. Black markers, mean ± SE; cells at higher MOI were binned together to allow for at least 10 cells per bin. Dashed line in pink, prediction by the MOI-independent model. Red curve, prediction by the MOI-dependent model. Data at 10 min following phage adsorption are shown. For other time points, see Figure S2.
See also Figure S2.

Please cite this article in press as: Nguyen et al., Coinfecting phages impede each other's entry into the cell, Current Biology (2024), https://doi.org/10.1016/j.cub.2024.05.032

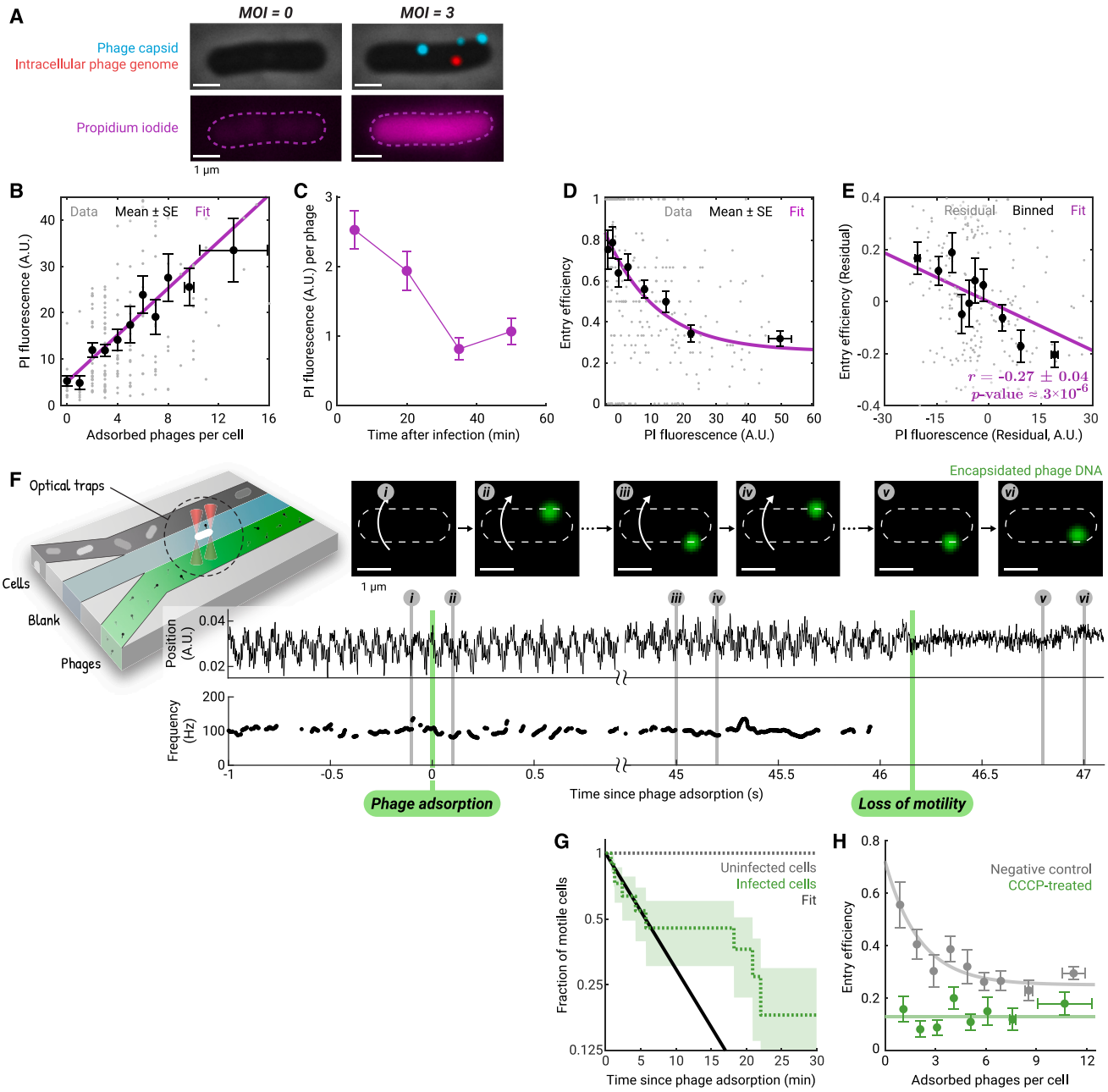

Figure 3. Phage adsorption causes cellular perturbation, resulting in impeded phage entry

(A) Following infection, cells were stained with propidium iodide (PI, shown in magenta). Dashed line, cell boundary. The image shown was taken 5 min after triggering genome ejection. Both cells were cropped from the same field of view. For additional cells, see Figure S4.

(B) Phages permeabilize the cell's membrane in an MOI-dependent manner. The intracellular fluorescence of PI is plotted as a function of the number of adsorbed phages. Gray markers, single-cell values (n = 188 cells). Black markers, mean ± SE; cells at higher MOI were binned together to allow for at least 10 cells per bin. Magenta line, linear fit, the slope of which reflects the degree of membrane permeabilization per phage. Data at 5 min after triggering genome ejection are shown. For other time points, see Figure S4.

(C) Infected cells recover membrane integrity. The slope of the linear fit between PI fluorescence and the number of adsorbed phages at each time point is plotted. Error bars indicate SE from bootstrapping (n = 188, 132, 131, and 135 cells).

(D) The efficiency of phage entry decreases in cells with stronger PI fluorescence. Gray markers, single-cell values (n = 298 cells pooled from t = 5 and 20 min). Black markers, mean ± SE (40 cells per bin). Magenta curve, fit to an exponential decay with a baseline.

(E) Phage entry efficiency and PI fluorescence, conditioned on the number of adsorbed phages, are negatively correlated. Gray markers, residuals obtained by linear regression of the PI fluorescence and of the entry efficiency on the number of adsorbed phages (n = 298 cells). Black markers, mean ± SE of the residuals (30 cells per bin). Magenta line, linear fit.

(F) The flagellar rotation frequency of phage-infected cells, indicating the membrane potential, is measured using optical traps. Top left: schematic of the trap setup and the flow chamber. Top right: a trapped cell with one adsorbed phage (encapsidated DNA was stained using SYTOX orange, shown in green), imaged

(legend continued on next page)

Please cite this article in press as: Nguyen et al., Coinfecting phages impede each other's entry into the cell, Current Biology (2024), https://doi.org/10.1016/j.cub.2024.05.032

perturbation increases with MOI[45,47] but does not always require phage entry to occur, as evidenced by infection of "ghost" phage particles devoid of DNA.[47–49] Could these perturbations to the host cell underlie the diminished entry we find at higher MOI? Consistent with this idea, ionic conditions have been shown to impact the kinetics of DNA ejection *in vitro*,[12] possibly by modulating the self-repulsion of the encapsidated DNA or altering the osmotic pressure that opposes ejection.[12] In lambda, specifically, both the extent[50–52] and rate[53,54] of DNA ejection are affected. Putting these elements together, we hypothesized that phage-induced perturbations to the host physiology, which occur following adsorption but prior to entry, impede phage entry into the cell in an MOI-dependent manner.

To directly probe the relation between phage-induced perturbation and DNA entry, we focused on two reported aspects of this perturbation: the compromise to membrane integrity and the reduction of membrane potential.[12] To measure the membrane integrity, we performed infection in LB supplemented with maltose and $MgSO_4$, sampled the infection mixture at different times, and stained cells using propidium iodide (PI; STAR Methods). For each cell, we recorded the numbers of adsorbed and intracellular phages, as well as the intracellular PI fluorescence (Figure 3A; see Figure S4 for additional cells). Within 5 min of infection, cells became permeable to PI, with intracellular PI fluorescence rising linearly with the number of adsorbed phages (Figure 3B). The MOI dependence of permeability is consistent with the idea that each adsorbed phage induces an opening in the cell membrane.[47,55] In agreement with reports that phage-induced perturbations do not require entry,[47,49] we found that PI permeation was not correlated with the intracellular phage numbers (Figure S4). We note that the permeation of PI into phage-infected cells did not reflect cell death or phage-induced lysis, and PI-stained cells still exhibited the sublinear relation between the numbers of adsorbed and intracellular phages (STAR Methods; Figure S4). Examining PI fluorescence later in infection, we found that the degree of PI permeation per adsorbed phage decreased over time, indicating that the infected cells gradually recover membrane integrity (Figure 3C). Taken together, these results show that phage adsorption transiently permeabilizes the infected cell's membrane in an MOI-dependent manner.

We next used the degree of PI permeation to test whether the compromise to membrane integrity impedes phage entry. Examining single-cell data up to 20 min post-infection (prior to the recovery of membrane integrity; Figure 3C), we found that cells with stronger PI fluorescence exhibited lower efficiency of phage entry (ratio of intracellular phage genomes to adsorbed phages per cell; Figure 3D). In particular, the entry efficiencies found in the least and most permeabilized cells were comparable to the values observed above for cells with low and high numbers of adsorbed phages, respectively (Figure 1C). Although these findings are consistent with the idea that the impediment to entry reflects the severity of the phage-induced perturbation, the observed correlation is vulnerable to the confounding effect of the number of adsorbed phages per cell, which is correlated with both the efficiency of phage entry (Figure 1C) and the intracellular PI fluorescence (Figure 3B). To directly establish the causal link between PI permeation and entry, we applied causal inference[56] by calculating the correlation between entry efficiency and PI fluorescence, conditioned on the number of adsorbed phages (STAR Methods; Figure S4). Consistent with our hypothesis, the correlation coefficient r(entry efficiency, PI fluorescence|number of adsorbed phages) was still negative (Figure 3E). Although we cannot rule out the presence of additional mechanisms connecting phage adsorption and impeded entry,[56] our causal inference analysis established that phage-induced compromise to membrane integrity is a cause of entry impediment.

To examine phage-induced changes to *E. coli*'s membrane potential, we utilized as proxies the flagellar rotation frequency[57] and the fluorescence of a proteo-rhodopsin optical proton sensor (PROPS),[58] both of which vary with the proton motive force. We used dual-trap optical tweezers to trap cells in a flow chamber, into which chemicals and phages can be perfused.[59] Trapped cells were fluorescently imaged, while their flagellar rotation frequency was inferred from the trap signal[60] (Figure 3F; STAR Methods). Exposing cells to carbonyl cyanide *m*-chlorophenyl hydrazone (CCCP), a protonophore that depletes the proton motive force,[58] resulted in rapid loss of flagellar motility and an increase in fluorescence from PROPS (Figure S5), as expected. A similar cessation of motility was exhibited following lambda adsorption (Figures 3F and 3G; Video S1). The typical time for an infected cell to lose motility—indicated by the half-life of the exponential fit in Figure 3G (5.7 ± 2.7 min; n = 11 cells, SE from bootstrapping)—was consistent with the timescale of ionic fluxes from lambda-infected cells (Figure S5).[43,46] The encapsidated DNA of the adsorbed phages could still be detected on cells that had lost motility (Figure 3F; Video S1), indicating that membrane depolarization did not require phage entry. Phage-induced depolarization was also revealed by the changes to PROPS fluorescence, which mirrored the effect of CCCP treatment (Figure S5).

Having established that lambda adsorption results in membrane depolarization, we next aimed to test whether membrane depolarization will in turn impede entry. To do so, we measured entry efficiency in cells treated with 200 μM CCCP (a concentration that induces a complete loss of membrane potential [Figure S5] and results in a similar degree of PI permeation to that

over time; the dashed line indicates the cell outline, and the white arrow indicates the cell body rotation. Bottom right: the trapped cell position and the flagellar rotation frequency of the same cell; gray vertical lines indicate the time points corresponding to the snapshots. See also Video S1.

(G) Phage adsorption results in loss of motility. Dotted green line, the fraction of motile cells following phage adsorption (MOI = 1), with shading for SE (n = 11 cells). Black line, exponential fit to the data up to 10 min. Dotted gray line, the fraction of motile cells in the uninfected sample (n = 7 cells).

(H) Complete membrane depolarization results in impeded phage entry. Green markers, mean (± SE) entry efficiency of cells depolarized using carbonyl cyanide *m*-chlorophenyl hydrazone (CCCP, n = 219 cells). Green line, the average over all cells in the CCCP-treated sample. Gray markers, mean ± SE for cells treated with 0.5% DMSO, serving as a negative control (n = 209 cells). Gray line, fit to an exponential decay with a baseline. For both samples, cells at higher MOI are binned together to allow for at least 5 cells per bin.

See also Figures S3–S5.

Please cite this article in press as: Nguyen et al., Coinfecting phages impede each other's entry into the cell, Current Biology (2024), https://doi.org/10.1016/j.cub.2024.05.032

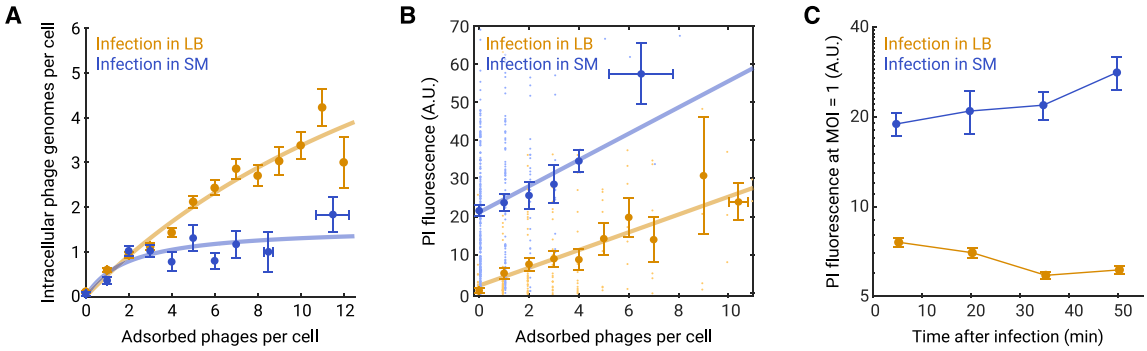

Figure 4. The infection medium modulates the extent of entry impediment

(A) Infection media alter the degree to which lambda entry is impeded. Identically cultured cells were infected in different media, and the numbers of adsorbed and intracellular phages per cell were measured at 5 min after triggering genome ejection. Orange markers, mean ± SE for infection in LB (data reproduced from Figure 1C). Blue markers, infection in SM (n = 242 cells, at least 5 cells per bin). Orange and blue curves, fit to a Michaelis-Menten function. For other infection media and buffers, see Figure S6.

(B) Membrane permeabilization in SM is more severe than that in LB. Light blue and light orange markers, single-cell values for the intracellular fluorescence of propidium iodide (PI) as a function of the number of adsorbed phages in the same cell, measured at 5 min after triggering genome ejection (n = 217 and 431 cells for LB and SM, respectively). Blue and orange markers, mean ± SE; cells at higher MOI were binned together to allow for at least 5 cells per bin. Blue and orange lines, linear fits.

(C) Membrane permeabilization in SM is longer-lasting than that in LB. The PI fluorescence in cells adsorbed by one phage (MOI = 1) was inferred from linear fitting of PI fluorescence as a function of the number of adsorbed phages, measured at different time points after triggering genome ejection. Orange markers, infection in LB (same time series data as shown in Figure S4). Blue markers, infection in SM (n = 261, 234, 190, and 184 cells at 5, 20, 35, and 50 min, respectively). Error bars indicate SE from bootstrapping.

See also Figure S6.

of lambda-infected cells [Figure S4]). Although intracellular lambda genomes were still detected following CCCP treatment, the entry efficiency (~15%, n = 219 cells) was lower than that of untreated cells (Figure 3H) and comparable to the value in (untreated) cells with high numbers of adsorbed phages (Figures 1C, 2F, and 3H). Depolarization-induced entry efficiency was also similar to that of highly permeabilized cells, as indicated by PI fluorescence (Figure 3D). Thus, CCCP-induced membrane depolarization emulates the perturbation caused by adsorption of multiple phages and results in significantly impeded phage entry.

The infection medium modulates the extent of entry impediment

Previous studies in several phages have shown that the severity and duration of phage-induced ionic perturbations strongly depend on the medium in which infection takes place.[61,62] In light of our finding that these perturbations underlie the MOI-dependent entry impediment, we reasoned that varying infection conditions would also result in different entry characteristics. To test this prediction, we grew cells in LB, supplemented with maltose and $MgSO_4$, and performed infection in 11 different solutions used in microbiological studies (STAR Methods). This survey revealed diverse relations between the numbers of adsorbed and intracellular phages (Figure S6). Some infection conditions, including LB, tryptone broth (TB), and M9 minimal media, permit multiple phage entries (Figure S6). However, under other conditions, such as saline magnesium (SM, a common phage buffer[63]), phosphate-buffered saline (PBS), and trap motility buffer (used in the optical trap assay[60]), adsorption by as many as ten or more phages only resulted, on average, in a single phage entry (Figure S6).

Taking SM as a representative of conditions where phage entry is severely impeded (Figure 4A), we confirmed that the compromise to the cell membrane in SM, measured using PI (STAR Methods), was more severe than that in LB (Figure 4B). Notably, the PI fluorescence in cells adsorbed by a single phage in SM was comparable to that induced by ~10 phages in LB (Figure 4B), at which point phage entry was strongly impeded. Furthermore, in contrast to LB where the PI fluorescence of singly adsorbed cells decreased over time (recall Figure 3C), the signal in SM *increased* (Figure 4C), suggesting that the phage-adsorbed cells in SM remain permeabilized at later times. Taken together, these results are consistent with the picture where the extent of entry impediment reflects the degree of phage-induced, medium-dependent perturbations.

Impediment to viral entry impacts the infection outcome

In nature, the occurrence of lysogeny is reported to vary greatly with the environmental conditions.[64,65] Motivated by the survey of infection media above (Figure S6), we hypothesized that the environmental conditions exert their influence on lysogeny, at least in part, by setting different limits on the intracellular phage number, which in turn drives the choice of developmental program by the phage.[8] To test this hypothesis, we assayed the frequency of lysogeny when infection takes place in the two media characterized above (Figure 4): LB (which enables multiple phage entries) and SM (which limits entry to a single phage, on average). In both cases, cell growth pre- and post-infection took place in LB,[8] and cells were not starved prior to infection (STAR Methods). Following Yao et al.[8], we again used a replication-deficient phage, where the number of viral genomes remains constant following entry. Under each infection condition, we measured the fraction of cells undergoing lysogeny as a

Please cite this article in press as: Nguyen et al., Coinfecting phages impede each other's entry into the cell, Current Biology (2024), https://doi.org/10.1016/j.cub.2024.05.032

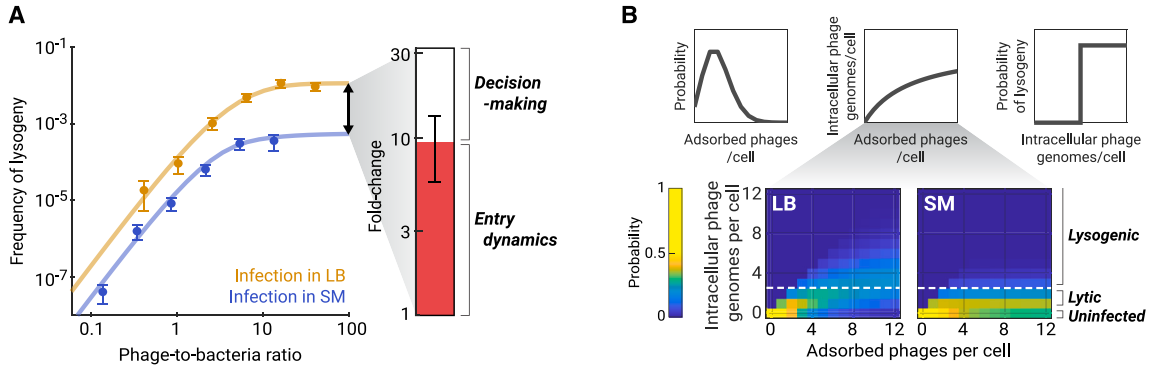

Figure 5. Impediment to viral entry impacts the infection outcome

(A) Entry dynamics in different media accounts for most of the difference in lysogenization frequency. Left: the frequencies of lysogeny as a function of phage-to-bacteria ratios (corrected for adsorption efficiency) when infection is performed in LB (orange) and SM (blue). Markers, mean ± SE from technical duplicates. Orange and blue curves, fit to the model in (B). Right: entry dynamics (red) accounts for ~10-fold of the observed ~30-fold difference in the maximum frequency of lysogeny between the two media. The other ~3-fold is due to differences in the single-cell probability of lysogeny (white, SE from bootstrapping).

(B) Schematic of the model used to capture the data in (A). Top: the model accounts for phage adsorption, entry, and decision-making. Bottom: the predicted distributions of intracellular phage numbers in LB and SM, parametrized using the data in Figure 4A. Dashed lines, the minimum MOI required for lysogenization. See also Figure S7 and Table S6.

function of the phage-to-bacteria ratio (Figure S7).[66] The two conditions resulted in distinct lysogeny-versus-MOI curves (Figure 5A). In particular, at higher ratios of phage to bacteria, when cells are likely absorbed by multiple phages, the frequency of lysogeny in SM saturated at a value ~30-fold lower than that in LB. Thus, given the same growth and recovery conditions, the choice of infection conditions dramatically impacted the propensity to lysogenize at high MOI.

We interpreted the lysogenization curves in the two media using a simple model (Figure 5B) consisting of (1) random phage-bacteria collisions, resulting in a Poisson distribution of single-cell numbers of adsorbed phages[8]; (2) stochastic entry of phages into the cell, parametrized using the experimentally measured values (Figures 4A and S6); and (3) choice of lysogeny if three or more phage genomes entered the cell[5,8] (STAR Methods). The model was able to capture the experimental curves (Figure 5A). The inferred model parameters revealed that the difference in phage entry—specifically, the reduced probability in SM of having three or more intracellular phages, even at high numbers of adsorbed phages—accounted for most of the difference in lysogenization between the two media (Figure 5A). In other words, when infecting in SM, the number of intracellular phage genomes poorly reflected the phage-to-bacteria ratio in the environment, resulting in a strong impact on infection outcome.

Protracted viral entry increases the heterogeneity in cell fate

Finally, beyond its impact on the lysogeny phenotype as measured in bulk (Figure 5), we asked whether entry dynamics can account for the reported cell-to-cell variability in infection outcome at a given MOI.[6,67,68] Although this heterogeneity has traditionally been attributed to the stochastic ("noisy") expression of genes in the decision network,[69] the idea lacks experimental evidence. We reasoned that, instead, the stochastic kinetics of phage entry may be key. This was motivated by recent works suggesting that, rather than simply measuring MOI, the lysis/lysogeny decision circuit weighs intracellular genomes by their arrival times, with latecomers contributing less to the outcome.[8,32] To test the consequences of stochastic entry, we first used our entry model (Figure 2B) to create simulated time series of phage entries in many individual cells, under varying numbers of adsorbed phages (STAR Methods). We then used this series as the input to a deterministic model of the decision network,[8] yielding the predicted kinetics for the concentrations of the Cro and CI transcription factors, and thus the infection outcome, in each cell (Figure 6A; see Figure S7 for additional MOIs). To facilitate comparison with the single-cell data of Zeng et al.,[6] we simulated infection by a replication-competent (wild-type) phage. When stochastic entry dynamics are ignored, i.e., all adsorbed phages are assumed to enter the cell instantaneously, cells adsorbed by two phages show dominant CI expression, resulting in the choice of lysogeny[8] (Figure 6A). By contrast, when entry dynamics is incorporated into the model, some cells adsorbed by two phages may have only one intracellular phage genome, or the second phage genome may arrive in the cell too late to contribute to the decision.[8,32] As a result, approx. 50% of the infected cells are Cro-dominant and will hence undergo lysis (Figure 6A; see Figure S7 for infection outcomes at other MOIs).

To quantify the heterogeneity in infection outcome, we calculated the resulting "decision curve," which describes the fraction of cells undergoing lysogeny as a function of single-cell MOI—here taken as the number of phages adsorbed to the cell, the observable in Zeng et al.[6] When entry dynamics were incorporated into the model, the predicted decision curve increased gradually rather than step-like, reminiscent of the data in Zeng et al.[6] (Figure 6B). The degree of precision of the decision can be quantified using the fitted Hill coefficient of this curve.[6,70] We found that incorporating entry dynamics into the model reduced the Hill coefficient from 7.9 ± 0.4 to 1.8 ± 0.1 (Figure 6B), thus considerably closer to the experimental value of 1.0 ± 0.1 in Zeng et al.[6] The "flattening" of the step-like response present in the original model[8] reflects the lower entry efficiency and slower

Please cite this article in press as: Nguyen et al., Coinfecting phages impede each other's entry into the cell, Current Biology (2024), https://doi.org/10.1016/j.cub.2024.05.032

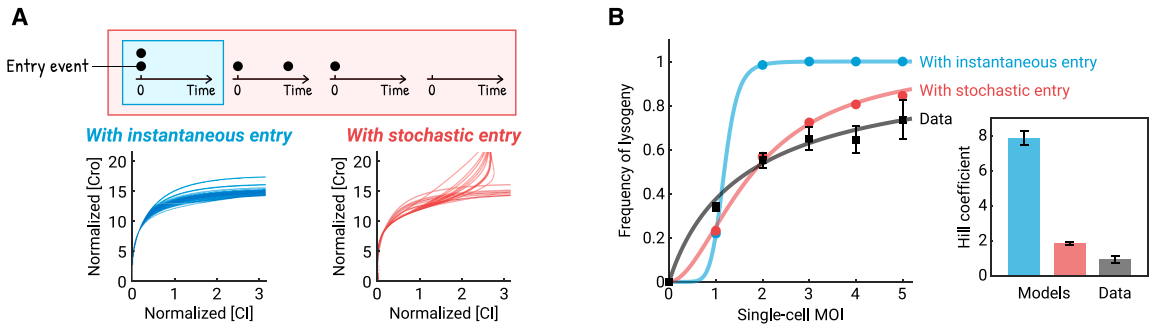

Figure 6. Protracted viral entry increases the heterogeneity in cell fate

(A) Stochastic phage entry results in different expression profiles of Cro (driving lysis) and CI (driving lysogeny). Top: schematics of the temporal change in the number of intracellular phage genomes in cells adsorbed by two phages, assuming instantaneous (cyan) or stochastic (red) phage entry. Bottom: predicted single-cell trajectories of Cro and CI concentrations in the Yao et al.[8] model, assuming different dynamics of phage entry. Trajectories of 24 cells, each adsorbed by two phages, are shown for each case. For other MOIs, see Figure S7.

(B) Entry dynamics increase the cell-to-cell variability in infection outcome at a given MOI. Black markers, data from Zeng et al.[6] Cyan and red markers, predictions by the model of Yao et al. in the absence or presence of stochastic entry kinetics, respectively. Solid curves, fits to Hill functions. The Hill coefficients, which describe the degree of precision in the lysis versus lysogeny decision, are shown on the right (SE from bootstrapping).

See also Figure S7.

entry in cells adsorbed by multiple phages. That this effect is captured by a fully deterministic model of the decision suggests a diminished role for stochastic gene expression in explaining the observed heterogeneity of outcome among cells.

Phages T5 and P1 exhibit MOI- and medium-dependent impediment to cell entry

Considering that phage-induced perturbations and ion-modulated ejection have been reported for multiple phage-bacteria systems,[12] we hypothesized that the MOI-dependent entry we found extends beyond lambda. We tested this hypothesis in two phages: T5, a virulent phage of the same *Siphoviridae* family as lambda, and P1, a temperate phage of the *Myoviridae* family. Motivating our choice, infections by both T5 and P1 have been reported to induce ionic fluxes and/or membrane depolarization.[43,71] To measure the efficiency of phage entry, we utilized the SYTOX orange assay (used above in lambda; Figure S1) and tracked the disappearance of fluorescently labeled encapsidated DNA in cells adsorbed by varying numbers of phages (Figure 7; STAR Methods). Mirroring the observation in lambda (Figures 1C and S1), we found that entry efficiency in both T5 and P1 decreased with the number of adsorbed phages (Figure 7). As in lambda (Figures 4A and S1), phage P1 exhibited lower entry efficiencies in SM than in LB (Figure 7). We were unable to quantify the entry efficiency of T5 in LB since some cells in the infected sample were already damaged—likely due to phage entry—by the time imaging began. This observation nevertheless suggested that T5 entry in LB was faster than that in SM. Taken together, these findings suggest that MOI-dependent impediment to entry, modulated by the infection medium, may be a general phenomenon.

DISCUSSION

Above, we provided evidence that phage-induced perturbations to the host cell impede DNA entry at high multiplicities of infection. However, the molecular details of this phenomenon remain unknown. Elucidating those details will contribute, we believe, to a deeper understanding of how phage entry takes place, including the forces driving DNA translocation and the structural changes to both phage particle and cell envelope during the entry process. Already, by highlighting the intimate relation between viral entry and the host's membrane integrity and ionic balance, our findings contribute to the emerging view of electrophysiology as a prime mover in the bacterial cell,[72] adding a role in phage infection to recent discoveries implicating electrophysiology in microbial stress response and biofilm formation.[73] More generally, our findings demonstrate yet again the importance of examining physiological processes in their native, *in vivo* context, where the full complexity of the cellular environment results in regulatory interactions absent from *in vitro* experiments.

The dynamics of viral entry, as described in this work, have important implications for the outcome of bacteriophage infection. For temperate phages, the strong dependence on medium conditions provides a way for the environment to impact the choice of cell fate by modulating the timing and number of phage genomes entering the cell. This previously unappreciated effect may help resolve the standing conflict between the simple MOI-to-lysogeny mapping observed in the lab and the complex, sometimes contradictory, relations found in natural phage habitats.[74–76] Beyond the case of infection by multiple copies of the same phage, mutual impedance of entry may facilitate competition between phages of different species that coinfect the same host,[77] where the effect may be seen as an alternative form of superinfection exclusion,[40,41] one that does not entail gene expression from the internalized phage genomes.

Finally, the stochastic and protracted entry of coinfecting phages may also have implications for the continuous arms race between phages and bacteria.[40,41] From the point of view of the infected cell, the sensitivity of phage entry to physiological parameters may provide an opportunity for the host to delay a critical step in the infection cycle, while its defenses are triggered,[46,78,79] and offers regulatory opportunities to halt this entry altogether. The reverse is that delayed entries may

Please cite this article in press as: Nguyen et al., Coinfecting phages impede each other's entry into the cell, Current Biology (2024), https://doi.org/10.1016/j.cub.2024.05.032

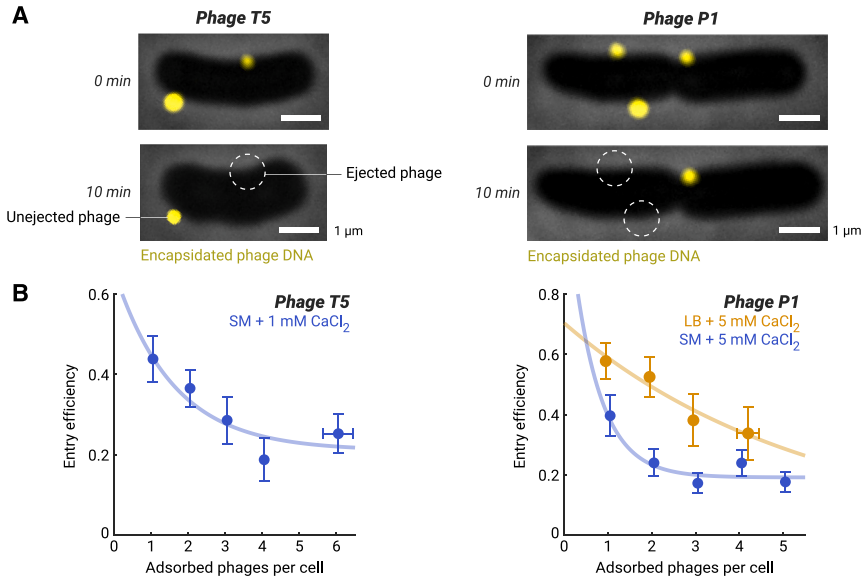

Figure 7. Phages T5 and P1 exhibit MOI- and medium-dependent impediment to cell entry

(A) *E. coli* cells infected by phages whose encapsidated DNA was fluorescently labeled using SYTOX orange (yellow signal). Left: infection by T5. Right: infection by P1. Dashed circles, the disappearance of SYTOX orange spots between 0 and 10 min was interpreted as ejection of the encapsidated DNA.

(B) Entry efficiency of phages T5 and P1 is reduced in cells adsorbed by multiple phages. Orange markers, mean ± SE for infection in LB (n = 234 cells for P1). Blue markers, mean ± SE for infection in SM (n = 256 and 221 cells for T5 and P1, respectively). For all samples, cells at higher MOI were binned together to allow for at least 5 cells per bin. Orange and blue curves, fits to an exponential decay with a baseline, serving as a guide to the eye. Both LB and SM were supplemented with $CaCl_2$, required for successful T5 and P1 infection.

facilitate cooperation between coinfecting phages, with early-arriving phages counteracting the host's defense system,[78,80] allowing later-arriving phages to survive and successfully propagate.[81]

STAR★METHODS

Detailed methods are provided in the online version of this paper and include the following:

SUPPLEMENTAL INFORMATION

Supplemental information can be found online at https://doi.org/10.1016/j.cub.2024.05.032.

ACKNOWLEDGMENTS

We are grateful to the following people for their generous advice: M. Gruebele, M. Goulian, C. Herman, K. Maxwell, I. Molineux, T. Pilizota, A. Sokac, K. Venken, T. Wensel, Z. Yu, C. Zong, and all members of the Golding lab. Work in the Golding lab is supported by the National Institutes of Health grant R35 GM140709, the National Science Foundation grant 2243257 (NSF Science and Technology Center for Quantitative Cell Biology), and the Alfred P. Sloan Foundation under grant G-2023-19649. Work in the Chemla lab is supported by the National Science Foundation Physics Frontiers Center (PFC) "Center for the Physics of Living Cells" (CPLC) grant PHY 1430124 and the National Institutes of Health grant R35 GM144125. Work in the Zeng lab is supported by the National Science Foundation grant MCB 2013762. We gratefully acknowledge the computing resources provided by the Computational and Integrative Biomedical Research Center of Baylor College of Medicine.

AUTHOR CONTRIBUTIONS

Conceptualization, T.V.P.N. and I.G.; methodology, T.V.P.N., Y.W., T.Y., J.T.T., L.Z., Y.R.C., and I.G.; investigation and formal analysis, T.V.P.N., Y.W., Y.R.C., and I.G.; visualization, T.V.P.N.; writing – original draft, T.V.P.N. and I.G.; writing – review & editing, T.V.P.N., L.Z., Y.R.C., and I.G.; funding acquisition and supervision, L.Z., Y.R.C., and I.G.; project administration, I.G.

DECLARATION OF INTERESTS

The authors declare no competing interests.

Received: August 11, 2023
Revised: February 15, 2024
Accepted: May 16, 2024
Published: June 14, 2024

REFERENCES

1. Oppenheim, A.B., Kobiler, O., Stavans, J., Court, D.L., and Adhya, S. (2005). Switches in bacteriophage lambda development. Annu. Rev. Genet. *39*, 409–429.
2. Casjens, S.R., and Hendrix, R.W. (2015). Bacteriophage lambda: early pioneer and still relevant. Virology *479–480*, 310–330.
3. Ofir, G., and Sorek, R. (2018). Contemporary phage biology: from classic models to new insights. Cell *172*, 1260–1270.
4. Shao, Q., Trinh, J.T., and Zeng, L. (2019). High-resolution studies of lysis–lysogeny decision-making in bacteriophage lambda. J. Biol. Chem. *294*, 3343–3349.
5. Kourilsky, P. (1973). Lysogenization by bacteriophage lambda. I. Multiple infection and the lysogenic response. Mol. Gen. Genet. *122*, 183–195.
6. Zeng, L., Skinner, S.O., Zong, C., Sippy, J., Feiss, M., and Golding, I. (2010). Decision making at a subcellular level determines the outcome of bacteriophage infection. Cell *141*, 682–691.
7. Weitz, J.S., Mileyko, Y., Joh, R.I., and Voit, E.O. (2008). Collective decision making in bacterial viruses. Biophys. J. *95*, 2673–2680.
8. Yao, T., Coleman, S., Nguyen, T.V.P., Golding, I., and Igoshin, O.A. (2021). Bacteriophage self-counting in the presence of viral replication. Proc. Natl. Acad. Sci. USA *118*, e2104163118.
9. Golding, I., Coleman, S., Nguyen, T.V.P., and Yao, T. (2020). Decision making by temperate phages. In Encyclopedia of Virology, Fourth Edition, *1–5*, D.H. Bamford, and M.B.T. Zuckerman, eds. (Academic Press), pp. 88–97.
10. Duddy, O.P., and Bassler, B.L. (2021). Quorum sensing across bacterial and viral domains. PLoS Pathog. *17*, e1009074.
11. Golding, I. (2018). Infection by bacteriophage lambda: an evolving paradigm for cellular individuality. Curr. Opin. Microbiol. *43*, 9–13.
12. Molineux, I.J., and Panja, D. (2013). Popping the cork: mechanisms of phage genome ejection. Nat. Rev. Microbiol. *11*, 194–204.
13. Chen, Y.J., Wu, D., Gelbart, W., Knobler, C.M., Phillips, R., and Kegel, W.K. (2018). Two-stage dynamics of in vivo bacteriophage genome ejection. Phys. Rev. X *8*, 021029.
14. Lemay, S.G., Panja, D., and Molineux, I.J. (2013). Role of osmotic and hydrostatic pressures in bacteriophage genome ejection. Phys. Rev. E Stat. Nonlin. Soft Matter Phys. *87*, 022714.
15. Schwartz, M. (1975). Reversible interaction between coliphage lambda and its receptor protein. J. Mol. Biol. *99*, 185–201.
16. Rothenberg, E., Sepúlveda, L.A., Skinner, S.O., Zeng, L., Selvin, P.R., and Golding, I. (2011). Single-virus tracking reveals a spatial receptor-dependent search mechanism. Biophys. J. *100*, 2875–2882.
17. Roa, M., and Scandella, D. (1976). Multiple steps during the interaction between coliphage lambda and its receptor protein in vitro. Virology *72*, 182–194.
18. Berrier, C., Bonhivers, M., Letellier, L., and Ghazi, A. (2000). High-conductance channel induced by the interaction of phage lambda with its receptor maltoporin. FEBS Lett. *476*, 129–133.
19. Wang, C., Duan, J., Gu, Z., Ge, X., Zeng, J., and Wang, J. (2024). Architecture of the bacteriophage lambda tail. Structure *32*, 35–46.e3.
20. Roessner, C.A., and Ihler, G.M. (1984). Proteinase sensitivity of bacteriophage lambda tail proteins gpJ and pH in complexes with the lambda receptor. J. Bacteriol. *157*, 165–170.
21. Esquinas-Rychen, M., and Erni, B. (2001). Facilitation of bacteriophage lambda DNA injection by inner membrane proteins of the bacterial phosphoenol-pyruvate: carbohydrate phosphotransferase system (PTS). J. Mol. Microbiol. Biotechnol. *3*, 361–370.
22. Cumby, N., Reimer, K., Mengin-Lecreulx, D., Davidson, A.R., and Maxwell, K.L. (2015). The phage tail tape measure protein, an inner membrane protein and a periplasmic chaperone play connected roles in the genome injection process of E. coli phage HK97. Mol. Microbiol. *96*, 437–447.
23. Scandella, D., and Arber, W. (1974). An Escherichia coli mutant which inhibits the injection of phage λ DNA. Virology *58*, 504–513.
24. Elliott, J., and Arber, W. (1978). E. coli K-12 pel mutants, which block phage λ DNA injection, coincide with ptsM, which determines a component of a sugar transport system. Mol. Gen. Genet. *161*, 1–8.
25. Scandella, D., and Arber, W. (1976). Phage λ DNA injection into Escherichia coli pel– mutants is restored by mutations in phage genes V or H. Virology *69*, 206–215.
26. Shao, Q., Hawkins, A., and Zeng, L. (2015). Phage DNA dynamics in cells with different fates. Biophys. J. *108*, 2048–2060.
27. Nielsen, H.J., Youngren, B., Hansen, F.G., and Austin, S. (2007). Dynamics of Escherichia coli chromosome segregation during multifork replication. J. Bacteriol. *189*, 8660–8666.
28. Tal, A., Arbel-Goren, R., Costantino, N., Court, D.L., and Stavans, J. (2014). Location of the unique integration site on an Escherichia coli chromosome by bacteriophage lambda DNA in vivo. Proc. Natl. Acad. Sci. USA *111*, 7308–7312.
29. Mackay, D.J., and Bode, V.C. (1976). Events in lambda injection between phage adsorption and DNA entry. Virology *72*, 154–166.
30. Dennehy, J.J., and Abedon, S.T. (2020). Adsorption: phage acquisition of bacteria. In Bacteriophages (Springer), pp. 1–25.
31. Moldovan, R., Chapman-McQuiston, E., and Wu, X.L. (2007). On kinetics of phage adsorption. Biophys. J. *93*, 303–315.
32. Cortes, M.G., Trinh, J.T., Zeng, L., and Balázsi, G. (2017). Late-arriving signals contribute less to cell-fate decisions. Biophys. J. *113*, 2110–2120.
33. Guan, J., Ibarra, D., and Zeng, L. (2019). The role of side tail fibers during the infection cycle of phage lambda. Virology *527*, 57–63.
34. Van Valen, D., Wu, D., Chen, Y.J., Tuson, H., Wiggins, P., and Phillips, R. (2012). A single-molecule Hershey-Chase experiment. Curr. Biol. *22*, 1339–1343.
35. Tzipilevich, E., Habusha, M., and Ben-Yehuda, S. (2017). Acquisition of phage sensitivity by bacteria through exchange of phage receptors. Cell *168*, 186–199.e12.
36. García, L.R., and Molineux, I.J. (1995). Rate of translocation of bacteriophage T7 DNA across the membranes of Escherichia coli. J. Bacteriol. *177*, 4066–4076.
37. Schwartz, M. (1976). The adsorption of coliphage lambda to its host: effect of variations in the surface density of receptor and in phage-receptor affinity. J. Mol. Biol. *103*, 521–536.
38. Plumbridge, J. (1998). Control of the expression of the manXYZ operon in Escherichia coli: Mlc is a negative regulator of the mannose PTS. Mol. Microbiol. *27*, 369–380.
39. Fraser, A.D.E., and Yamazaki, H. (1983). Regulatory relationship between PTSM and PTSG in Escherichia coli. FEMS Microbiol. Lett. *16*, 61–63.
40. Labrie, S.J., Samson, J.E., and Moineau, S. (2010). Bacteriophage resistance mechanisms. Nat. Rev. Microbiol. *8*, 317–327.
41. Hampton, H.G., Watson, B.N.J., and Fineran, P.C. (2020). The arms race between bacteria and their phage foes. Nature *577*, 327–336.
42. Wang, M., Zhang, J., Xu, H., and Golding, I. (2019). Measuring transcription at a single gene copy reveals hidden drivers of bacterial individuality. Nat. Microbiol. *4*, 2118–2127.
43. Kuhn, A., and Kellenberger, E. (1985). Productive phage infection in Escherichia coli with reduced internal levels of the major cations. J. Bacteriol. *163*, 906–912.
44. Letellier, L., Plançon, L., Bonhivers, M., and Boulanger, P. (1999). Phage DNA transport across membranes. Res. Microbiol. *150*, 499–505.
45. Kourilsky, P., and Knapp, A. (1974). Lysogenization by bacteriophage lambda. III. Multiplicity dependent phenomena occuring upon infection by lambda. Biochimie *56*, 1517–1523.
46. Kronheim, S., Daniel-Ivad, M., Duan, Z., Hwang, S., Wong, A.I., Mantel, I., Nodwell, J.R., and Maxwell, K.L. (2018). A chemical defence against phage infection. Nature *564*, 283–286.

47. Boulanger, P., and Letellier, L. (1988). Characterization of ion channels involved in the penetration of phage T4 DNA into Escherichia coli cells. J. Biol. Chem. *263*, 9767–9775.

48. Duckworth, D.H. (1970). Biological activity of bacteriophage ghosts and "take-over" of host functions by bacteriophage. Bacteriol. Rev. *34*, 344–363.

49. Duckworth, D.H., and Winkler, H.H. (1972). Metabolism of T4 bacteriophage ghost-infected cells. II. Do ghosts cause a generalized permeability change? J. Virol. *9*, 917–922.

50. Filali Maltouf, A.K., and Labedan, B. (1985). The energetics of the injection process of bacteriophage lambda DNA and the role of the ptsM pel-encoded protein. Biochem. Biophys. Res. Commun. *130*, 1093–1101.

51. Evilevitch, A., Lavelle, L., Knobler, C.M., Raspaud, E., and Gelbart, W.M. (2003). Osmotic pressure inhibition of DNA ejection from phage. Proc. Natl. Acad. Sci. USA *100*, 9292–9295.

52. Jeembaeva, M., Castelnovo, M., Larsson, F., and Evilevitch, A. (2008). Osmotic pressure: resisting or promoting DNA ejection from phage? J. Mol. Biol. *381*, 310–323.

53. Wu, D., Van Valen, D., Hu, Q., and Phillips, R. (2010). Ion-dependent dynamics of DNA ejections for bacteriophage λ. Biophys. J. *99*, 1101–1109.

54. Li, D., Liu, T., Zuo, X., Li, T., Qiu, X., and Evilevitch, A. (2015). Ionic switch controls the DNA state in phage λ. Nucleic Acids Res. *43*, 6348–6358.

55. Roessner, C.A., and Ihler, G.M. (1986). Formation of transmembrane channels in liposomes during injection of λ DNA. J. Biol. Chem. *261*, 386–390.

56. Kar, P., Tiruvadi-Krishnan, S., Männik, J., Männik, J., and Amir, A. (2023). Using conditional independence tests to elucidate causal links in cell cycle regulation in Escherichia coli. Proc. Natl. Acad. Sci. USA *120*, e2214796120.

57. Gabel, C.V., and Berg, H.C. (2003). The speed of the flagellar rotary motor of Escherichia coli varies linearly with protonmotive force. Proc. Natl. Acad. Sci. USA *100*, 8748–8751.

58. Kralj, J.M., Hochbaum, D.R., Douglass, A.D., and Cohen, A.E. (2011). Electrical spiking in Escherichia coli probed with a fluorescent voltage-indicating protein. Science *333*, 345–348.

59. Min, T.L., Mears, P.J., Golding, I., and Chemla, Y.R. (2012). Chemotactic adaptation kinetics of individual Escherichia coli cells. Proc. Natl. Acad. Sci. USA *109*, 9869–9874.

60. Min, T.L., Mears, P.J., Chubiz, L.M., Rao, C.V., Golding, I., and Chemla, Y.R. (2009). High-resolution, long-term characterization of bacterial motility using optical tweezers. Nat. Methods *6*, 831–835.

61. Keweloh, H.W., and Bakker, E.P. (1984). Increased permeability and subsequent resealing of the host cell membrane early after infection of Escherichia coli with bacteriophage T1. J. Bacteriol. *160*, 354–359.

62. Bonhivers, M., and Letellier, L. (1995). Calcium controls phage T5 infection at the level of the Escherichia coli cytoplasmic membrane. FEBS Lett. *374*, 169–173.

63. Sambrook, J., and Russell, D.; Cold Spring Harbor Laboratory (2001). Molecular Cloning: A Laboratory Manual, Third Edition, D.W. Russell, ed. (Cold Spring Harbor Laboratory).

64. Howard-Varona, C., Hargreaves, K.R., Abedon, S.T., and Sullivan, M.B. (2017). Lysogeny in nature: mechanisms, impact and ecology of temperate phages. ISME J. *11*, 1511–1520.

65. Luque, A., and Silveira, C.B. (2020). Quantification of lysogeny caused by phage coinfections in microbial communities from biophysical principles. mSystems *5*, e00353-20.

66. Geng, Y., Nguyen, T.V.P., Homaee, E., and Golding, I. (2023). Using population dynamics to count bacteriophages and their lysogens. Preprint at bioRxiv. https://doi.org/10.1101/2023.10.06.561271.

67. Lieb, M. (1953). The establishment of lysogenicity in Escherichia coli. J. Bacteriol. *65*, 642–651.

68. St-Pierre, F., and Endy, D. (2008). Determination of cell fate selection during phage lambda infection. Proc. Natl. Acad. Sci. USA *105*, 20705–20710.

69. Arkin, A., Ross, J., and McAdams, H.H. (1998). Stochastic kinetic analysis of developmental pathway bifurcation in phage λ-infected Escherichia coli cells. Genetics *149*, 1633–1648.

70. Alon, U. (2019). An Introduction to Systems Biology: Design Principles of Biological Circuits, Second Edition (CRC Press).

71. Boulanger, P., and Letellier, L. (1992). Ion channels are likely to be involved in the two steps of phage T5 DNA penetration into Escherichia coli cells. J. Biol. Chem. *267*, 3168–3172.

72. Benarroch, J.M., and Asally, M. (2020). The microbiologist's guide to membrane potential dynamics. Trends Microbiol. *28*, 304–314.

73. Galera-Laporta, L., Comerci, C.J., Garcia-Ojalvo, J., and Süel, G.M. (2021). IonoBiology: The functional dynamics of the intracellular metallome, with lessons from bacteria. Cell Syst. *12*, 497–508.

74. Chevallereau, A., Pons, B.J., van Houte, S., and Westra, E.R. (2022). Interactions between bacterial and phage communities in natural environments. Nat. Rev. Microbiol. *20*, 49–62.

75. Correa, A.M.S., Howard-Varona, C., Coy, S.R., Buchan, A., Sullivan, M.B., and Weitz, J.S. (2021). Revisiting the rules of life for viruses of microorganisms. Nat. Rev. Microbiol. *19*, 501–513.

76. Silveira, C.B., Luque, A., and Rohwer, F. (2021). The landscape of lysogeny across microbial community density, diversity and energetics. Environ. Microbiol. *23*, 4098–4111.

77. Koskella, B., Hernandez, C.A., and Wheatley, R.M. (2022). Understanding the impacts of bacteriophage viruses: from laboratory evolution to natural ecosystems. Annu. Rev. Virol. *9*, 57–78.

78. García, L.R., and Molineux, I.J. (1999). Translocation and specific cleavage of bacteriophage T7 DNA in vivo by EcoKI. Proc. Natl. Acad. Sci. USA *96*, 12430–12435.

79. Modell, J.W., Jiang, W., and Marraffini, L.A. (2017). CRISPR-Cas systems exploit viral DNA injection to establish and maintain adaptive immunity. Nature *544*, 101–104.

80. Borges, A.L., Zhang, J.Y., Rollins, M.F., Osuna, B.A., Wiedenheft, B., and Bondy-Denomy, J. (2018). Bacteriophage cooperation suppresses CRISPR-Cas3 and Cas9 immunity. Cell *174*, 917–925.e10.

81. Landsberger, M., Gandon, S., Meaden, S., Rollie, C., Chevallereau, A., Chabas, H., Buckling, A., Westra, E.R., and van Houte, S. (2018). Anti-CRISPR phages cooperate to overcome CRISPR-Cas immunity. Cell *174*, 908–916.e12.

82. Schindelin, J., Arganda-Carreras, I., Frise, E., Kaynig, V., Longair, M., Pietzsch, T., Preibisch, S., Rueden, C., Saalfeld, S., Schmid, B., et al. (2012). Fiji: an open-source platform for biological-image analysis. Nat. Methods *9*, 676–682.

83. Sanders, E.R. (2012). Aseptic laboratory techniques: plating methods. J. Vis. Exp. *63*, e3064.

84. Zeng, L., and Golding, I. (2011). Following cell-fate in E. coli after infection by phage lambda. J. Vis. Exp. *56*, e3363.

85. Zhang, K., Young, R., and Zeng, L. (2020). Bacteriophage P1 does not show spatial preference when infecting Escherichia coli. Virology *542*, 1–7.

86. Nielsen, H.J., Li, Y., Youngren, B., Hansen, F.G., and Austin, S. (2006). Progressive segregation of the Escherichia coli chromosome. Mol. Microbiol. *61*, 383–393.

87. Cohen, D., Melamed, S., Millman, A., Shulman, G., Oppenheimer-Shaanan, Y., Kacen, A., Doron, S., Amitai, G., and Sorek, R. (2019). Cyclic GMP–AMP signalling protects bacteria against viral infection. Nature *574*, 691–695.

88. Skinner, S.O., Sepúlveda, L.A., Xu, H., and Golding, I. (2013). Measuring mRNA copy number in individual Escherichia coli cells using single-molecule fluorescent in situ hybridization. Nat. Protoc. *8*, 1100–1113.

89. Yang, Y., Karin, O., Mayo, A., Song, X., Chen, P., Santos, A.L., Lindner, A.B., and Alon, U. (2023). Damage dynamics and the role of chance in the timing of E. coli cell death. Nat. Commun. *14*, 2209.

90. Brooks, K. (1965). Studies in the physiological genetics of some suppressor-sensitive mutants of bacteriophage λ. Virology *26*, 489–499.

91. Mears, P.J., Koirala, S., Rao, C.V., Golding, I., and Chemla, Y.R. (2014). Escherichia coli swimming is robust against variations in flagellar number. eLife *3*, e01916.

92. Leavitt, J.C., Gogokhia, L., Gilcrease, E.B., Bhardwaj, A., Cingolani, G., and Casjens, S.R. (2013). The tip of the tail needle affects the rate of DNA delivery by bacteriophage P22. PLoS One *8*, e70936.

93. Reichardt, L.F. (1975). Control of bacteriophage lambda repressor synthesis after phage infection: The role of the N, cII, cIII and cro products. J. Mol. Biol. *93*, 267–288.

94. Kobiler, O., Rokney, A., Friedman, N., Court, D.L., Stavans, J., and Oppenheim, A.B. (2005). Quantitative kinetic analysis of the bacteriophage λ genetic network. Proc. Natl. Acad. Sci. USA *102*, 4470–4475.

95. Papoulis, A. (1991). Probability, Random Variables, and Stochastic Processes (McGraw-Hill).

96. Arfken, G.B., Weber, H.J., and Harris, F.E. (2013). Mathematical Methods for Physicists: A Comprehensive Guide (Elsevier Science).

97. Grayson, P., Evilevitch, A., Inamdar, M.M., Purohit, P.K., Gelbart, W.M., Knobler, C.M., and Phillips, R. (2006). The effect of genome length on ejection forces in bacteriophage lambda. Virology *348*, 430–436.

98. Nurmemmedov, E., Castelnovo, M., Medina, E., Catalano, C.E., and Evilevitch, A. (2012). Challenging packaging limits and infectivity of phage λ. J. Mol. Biol. *415*, 263–273.

99. Gillespie, D.T. (2007). Stochastic simulation of chemical kinetics. Annu. Rev. Phys. Chem. *58*, 35–55.

Please cite this article in press as: Nguyen et al., Coinfecting phages impede each other's entry into the cell, Current Biology (2024), https://doi.org/10.1016/j.cub.2024.05.032

STAR★METHODS

KEY RESOURCES TABLE

REAGENT or RESOURCE	SOURCE	IDENTIFIER
Bacterial and virus strains		
E. coli MG1655, wild-type	Lab stock	N/A
E. coli LE392, *glnV* (*supE*44) *tryT* (*supF*58)	Lab stock	N/A
Phage lambda, λ_{TY11} (λ *cI*857 *Pam*80 *stf*::P1*parS-kan*^{R})	Lab stock; see Yao et al.[8]	N/A
Phage lambda, λ_{TY8} (λ *cI*857 *stf*::P1*parS-kan*^{R})	Lab stock	N/A
Phage T5	Coli Genetic Stock Center	# 12144
Phage P1*vir*	Lab stock	N/A
Chemicals, peptides, and recombinant proteins		
Ampicillin	Fisher Scientific	# BP1760-25
Kanamycin	Fisher Scientific	# BP906-5
NaCl	Fisher Scientific	# BP358-1
NaOH	Fisher Scientific	# BP359-500
$MgSO_4$	Fisher Scientific	# BP213-1
$CaCl_2$	Fisher Scientific	# BP510-500
Tris-Cl	Fisher Scientific	# BP152-500
K_2HPO_4	EMD Millipore	# PX1570-1
KH_2PO_4	EMD Millipore	# PX1565-1
EDTA	Promega Life Sciences	# V4231
Maltose	Fisher Scientific	# BP684-500
Glucose	Fisher Scientific	# BP350-500
L-arabinose	Sigma-Aldrich	# A3256
Glycerol	Fisher Scientific	# BP229
Isopropyl-β-thiogalactoside (IPTG)	Sigma-Aldrich	# I6758
Carbonyl cyanide *m*-chlorophenyl hydrazone (CCCP)	Acros Organics	# AC228131000 (Thermo Scientific Chemicals)
Rifampicin	Fisher Scientific	# BP26795
SYTOX Orange	Invitrogen	# S11368
4′,6-diamidino-2-phenylindole (DAPI)	Invitrogen	# D1306
All-*trans* retinal	Sigma-Aldrich	# R2500
Propidium iodide (PI)	Invitrogen	# P1304MP
Pyranose oxidase	Sigma-Aldrich	# P4234
Catalase	EMD Millipore	# 219261
Agar	BD Biosciences	# 214010
Agarose	Sigma-Aldrich	# A9414
Tryptone	Gibco	# 211705 (Thermo Fisher Scientific)
Yeast extract	Gibco	# 212750 (Thermo Fisher Scientific)
NZYM	Teknova	# N2062
M9 minimal salts broth without carbon source	Teknova	# M8005
M9 minimal salt broth with 1% glucose and 0.1% casamino acids	Teknova	# M8010
SM	Teknova	# S0249
10× PBS	Invitrogen	# AM9624
Formaldehyde	Fisher Scientific	# BP531-500
Ethanol	Decon Labs	# 2716
Dimethyl sulfoxide (DMSO)	Fisher Scientific	# BP231-100

(*Continued on next page*)

Please cite this article in press as: Nguyen et al., Coinfecting phages impede each other's entry into the cell, Current Biology (2024), https://doi.org/10.1016/j.cub.2024.05.032

Continued

REAGENT or RESOURCE	SOURCE	IDENTIFIER
Recombinant DNA		
p2973 (P_{trc}-mCherry-P1Δ30ParB-YGFP-pMT1Δ23ParB)	Tal et al.[28]	N/A
pALA3047 (P_{trc}-CFP-P1Δ30ParB)	Gift of Stuart Austin; see also, Yao et al.[8]	N/A
pACYC177-P_{late}*D-mTurquoise2	Shao et al.[26]	N/A
pACYC177-P_{late}*D-EYFP	Shao et al.[26]	N/A
pJMK001 (P_{araBAD}-PROPS)	Kralj et al.[58]	# 33780 (Addgene)
Software and algorithms		
Original MATLAB scripts for simulating phage entry and infection outcome	This study	https://github.com/thuvpnguyen/
NIS-Elements	Nikon	https://www.nikon.com/
ImageJ2/FIJI	Schindelin et al.[82]	https://imagej.net/
Mathematica	Wolfram	https://wolfram.com/
MATLAB	MathWorks	https://www.mathworks.com/
Other		
Slide-A-Lyzer MINI Dialysis Devices, 2K MWCO	Thermo Scientific	# 69580
22×22 mm coverslips no. 1	Fisherbrand	# 12-542-BP
24×50 mm coverslips no. 1	Fisherbrand	# 12-545-FP
CellASIC ONIX and ONIX2 microfluidic systems (see STAR Methods for details)	Millipore Sigma	N/A
Epifluorescence microscope systems (see STAR Methods for details)	Nikon and others	N/A
Optical trap system (see STAR Methods for details)	Various	N/A
Microplates and microplate readers (see STAR Methods for details)	TECAN and others	N/A
Equipment for standard procedures in microbiology and molecular biology (see STAR Methods for details)	Various	N/A

RESOURCE AVAILABILITY

Lead contact

Requests for further information, resources, or reagents should be directed to and will be fulfilled by the lead contact, Ido Golding (igolding@illinois.edu).

Materials availability

This study did not generate new unique reagents.

Data and code availability

- All data reported in this paper will be shared by the lead contact upon request.
- The original code for simulating phage entry and infection outcome has been deposited at https://github.com/thuvpnguyen/ and is publicly available as of the date of publication (see also, the key resources table).
- Any additional information required to reanalyze the data reported in this paper is available from the lead contact upon request.

EXPERIMENTAL MODEL AND SUBJECT DETAILS

Bacterial strains, phages, and plasmids

All strains and plasmids used in this study are listed in the key resources table and Table S1. The lambda strain used in this study, λ_{TY11} (λ *cI*857 *Pam*80 *stf*::P1*parS-kan*^{R}),[8] is unable to replicate in wild-type (MG1655) host. Capsids of the infecting phages were labeled using gpD-mTurquoise2 or gpD-EYFP fusions.[26] Intracellular phage genomes, each harboring a *parS* sequence, were labeled using mCherry-ParB or CFP-ParB fusions.[8,28] Plasmid transformation (using a Bio-Rad MicroPulser Electroporator), colony plating, and phage titering followed standard protocols.[63,83]

Please cite this article in press as: Nguyen et al., Coinfecting phages impede each other's entry into the cell, Current Biology (2024), https://doi.org/10.1016/j.cub.2024.05.032

Chemical reagents, growth media, and buffers

Reagents used in sections "phage preparation", "bacterial growth conditions", and in method details below are listed in the key resources table and Table S2, excluding those involved in the phage purification protocol (following Zeng and Golding[84]) and those involved in section "optical trap assay" (following Min et al.[60]). Growth media and buffers used in this study are described in Table S3. The growth medium in most experiments was LB (Lennox formulation).[63] The medium in optical trap experiments was tryptone broth (TB).[60] Plaque assays to titer phages were performed using NZYM.[8,84] Supplements to growth media are specified below for each experiment. Agar plates and soft agar were prepared by supplementing the medium with 1.5% and 0.7% (w/v) agar, respectively. All media were autoclaved at 121°C for at least 25 minutes in a liquid cycle for sterilization.

Phage preparation

Production and purification of lambda phages

This procedure was performed as described in Zeng and Golding.[84] Briefly, fluorescently labeled phages were produced from LE392 λ_{TY11} lysogens harboring plasmids that express gpD-mTurquoise2 or gpD-EYFP. Crude phage lysates were obtained using heat induction, followed by precipitation using polyethylene glycol (PEG), CsCl ultracentrifugation, and dialysis into SM buffer. For the ultracentrifugation step, the step and equilibrium gradients were both set up using 14 mL ultracentrifuge tubes, and spun at 4°C using a Beckman SW40Ti rotor for 4–6 hours at 24,000 rpm, or 20–24 hours at 35,000 rpm, respectively.

The concentration of the purified phage stock (typically 10^{11}–10^{12} plaque-forming units [PFU]/mL) was measured using LE392 indicator cells. To measure the efficiency of capsid labeling, the phages were stained using 5 μg/mL DAPI.[84] Then, 1 μL of stained phages was mounted between a 24×50 mm coverslip no. 1 and a 22×22 mm coverslip no. 1, and imaged as described in section "microscopy". The efficiency of capsid labeling is defined to be the fraction of detected phages with both capsid and DAPI signals (97.0 ± 1.0%, mean and standard error, SE, from 3 independent phage purification runs, Figure S1A).

Production of other phages

Phages T5 and P1 were produced by performing infection of liquid cell cultures.[63] Briefly, cultures of MG1655 were grown in LB (supplemented with 1 mM $CaCl_2$ for T5,[62] or 5 mM $CaCl_2$ for P1[85]) at 37°C with aeration. When the culture reached the optical density (OD_{600}) ≈ 0.2, approx. 10^7 PFU of phage T5 or P1 were added to the cultures, and the cell cultures were incubated at 37°C without shaking for 15 minutes. Shaking was then resumed, and the OD was monitored until lysis was observed. The phage lysates were treated with 5% chloroform, incubated at room temperature (RT) for 20 minutes, and centrifuged at 4500×g for 10 minutes at 4°C. The clear supernatants were transferred to new Corning tubes and stored with 0.3% chloroform at 4°C.

SYTOX Orange staining

In some experiments, phage particles were stained with SYTOX Orange, a DNA-intercalating fluorescent dye, following the protocols from Van Valen et al.[34] and Tzipilevich et al.[35] The phage stock of lambda, T5, or P1 was first diluted into the same medium or buffer as the subsequent infection step. Phages were mixed with 500 nM SYTOX Orange and incubated in the dark at RT for 3 hours. Excess SYTOX Orange was removed using Slide-A-Lyzer MINI Dialysis Devices (2K MWCO, ThermoScientific) in two rounds of dialysis, each round for 2 hours at RT in at least 500× the phage volume. Staining and dialysis were always performed on the day of infection.

To estimate the efficiency of SYTOX Orange labeling in phage lambda, the stained phages were mounted as described above for DAPI staining and imaged as described in section "microscopy". The labeling efficiency is defined to be the fraction of detected capsids with colocalized SYTOX Orange signal (91.9% ± 1.6%, mean and SE from 3 independent staining replicates, Figure S1B).

Bacterial growth conditions

Equipment

Bacterial agar plates were incubated in Isotemp Microbiological Incubators (Fisherbrand). Liquid cultures were grown with aeration (using 220 rpm shaking) in either a MaxQ 4000 Benchtop Orbital Shaker (Thermo Scientific), a MaxQ 7000 Water Bath Orbital Shaker (Thermo Scientific), or an Excella E24 Incubator Shaker (New Brunswick Scientific, Eppendorf). Optical density (OD) was measured using a SmartSpec Plus spectrophotometer (Bio-Rad).

Plating and overnight cultures

Cells were streaked from 15% glycerol stocks (stored at -80°C) onto LB agar plates (supplemented with 100 μg/mL ampicillin and/or 50 μg/mL kanamycin when applicable) and incubated at 30°C for approx. 16 hours. For overnight cultures, fresh colonies were inoculated into 2 mL of growth medium (supplemented with antibiotics at the same concentration as the agar plates when applicable) in 14 mL round-bottom test tubes (Falcon). Overnight cultures were grown for approx. 16 hours at 30°C with aeration.

Experimental cultures

To prepare cells expressing mCherry-ParB or CFP-ParB (MG1655 harboring p2973 or pALA3047), we followed the protocol of Yao et al.[8] Experimental cultures ("overday" cultures) were prepared by diluting the overnight cultures by at least 1:500 into LBMM (for most experiments), LBGM, M9Mal, M9Glu, or TBM, all supplemented with IPTG, in baffled Erlenmeyer flasks; the culture volume (typically 12 mL) was 10–20% of the flask volume. The medium was supplemented with 100 μM or 10 μM IPTG to induce the expression of mCherry-ParB or CFP-ParB from p2973 or pALA3047, respectively. We note that inducing p2973 using 10 μM IPTG resulted in poor fluorescence, whereas inducing pALA3047 using 100 μM IPTG may result in aggregates.[86] The cultures were grown at 37°C with aeration to OD_{600} ≈ 0.3–0.4 and harvested as described for each experiment below in method details.

To prepare cells expressing the proteorhodopsin optical proton sensor (PROPS) for all experiments except for those in section "optical trap assay", we followed the protocol of Kralj et al.[58] Cultures of MG1655 harboring pJMK001 were grown in LB at 33°C

Please cite this article in press as: Nguyen et al., Coinfecting phages impede each other's entry into the cell, Current Biology (2024), https://doi.org/10.1016/j.cub.2024.05.032

with aeration. When the culture reached $OD_{600} \approx 0.3$, 0.2% L-arabinose (for P_{araBAD} induction) and 5 μM all-*trans* retinal (the chromophore of PROPS) were added to the cultures. Growth was resumed in the dark for 3 hours, after which the cultures were harvested as described in section "validating the CCCP treatment protocol using PROPS". We note that MG1655 harboring pJMK001, when cultured with 10 mM $MgSO_4$, showed no detectable PROPS fluorescence. Hence, $MgSO_4$ was omitted during growth and only supplemented before the infection step to enable phage adsorption.[31] Because PROPS is expressed from an arabinose-induced promoter, we also omitted maltose to avoid interference with arabinose uptake. Previous studies have shown that adsorption of lambda phages still occurred in the absence of maltose in the growth medium[31,36] (also confirmed in this work, Figure S3A).

To prepare motile cells for experiments in section "optical trap assay", we followed the protocol of Min et al.[60] Cultures of MG1655 or MG1655 harboring pJMK001 (expressing PROPS) were grown in TB at 30°C with aeration. For MG1655, the cultures were harvested upon reaching $OD_{600} \approx 0.5$ as described below. For MG1655 harboring pJMK001, induction of PROPS was performed as described above.

To prepare cells for experiments in sections "potassium efflux assay" and "measuring the frequency of lysogeny following infection in different media", cultures of MG1655 were grown in LBMM and LBM, respectively, at 37°C with aeration, and harvested upon reaching $OD_{600} \approx 0.3$–0.4 as described below.

METHOD DETAILS

Measuring the numbers of adsorbed phages and intracellular phage genomes following bulk infection

Preparation of cells and phages

Cultures of MG1655 harboring p2973 or pALA3047 were grown at 37°C in LBMM (for most experiments), LBGM, M9Mal, M9Glu, or TBM, supplemented with IPTG as described in section "bacterial growth conditions". When the cultures reached $OD_{600} \approx 0.3$–0.4, 10 mL of cells were transferred to a centrifuge tube (Corning) and spun at 2000×g for 10 minutes at 4°C using a Thermo Scientific Sorvall Legend XTR centrifuge, and the supernatant was removed. The cell pellet was resuspended in 1 mL of an ice-cold medium or buffer (dictated by the subsequent infection step) and transferred to a 1.5 mL microcentrifuge tube (Eppendorf). The cell suspension was centrifuged at 21,130×g for 30 seconds at RT using an Eppendorf 5420 centrifuge, and the supernatant was removed. The cell pellet was resuspended in 100 μL of the ice-cold medium or buffer and used for infection immediately.

The purified phage stock (λ_{TY11} with fluorescently labeled capsids, described in section "phage preparation") was diluted to 2×10^{10} PFU/mL using the same medium or buffer as the cell resuspension. In most experiments, gpD-mTurquoise2 phages were used to infect MG1655 harboring p2973 (expressing mCherry-ParB). In some experiments, including those involving SYTOX Orange, gpD-EYFP phages were used to infect MG1655 harboring pALA3047 (CFP-ParB).

Infection

Infection mixtures comprising 10 μL of cells and 10 μL of phages (with phage-to-bacteria ratio ≈ 3), and a negative (uninfected) control comprising cells and blank solution were prepared. In experiments where the phage-to-bacteria ratio was varied (Figure 1B), phages at different concentrations were used but the volume ratio between cells and phages remained constant. The samples were cooled at 4°C for 30 minutes in a dry block incubator (ThermoFisher/VWR) to allow phages to adsorb to cells, then heated at 35°C for 5 minutes to trigger phage ejection. Using wide pipette tips, the samples were gently diluted 1:10 to decrease the cell density before imaging. During this step, if the infection medium was based on LB or TB, we used PBSM for dilution to reduce the autofluorescence background.[16] Otherwise, the same solution as the infection step was used for dilution.

Sample mounting and imaging

Samples were mounted for imaging as described in Zeng et al.[6] Briefly, a 1.5% agarose pad (made using the same solution as the one used to dilute the infection mixture) was laid on top of a 22×22 mm coverslip no. 1. Then, using a wide pipette tip, 1 μL of the diluted sample was gently pipetted onto the pad. When the 1 μL droplet was no longer visible (1–2 minutes), a 24×50 mm coverslip no. 1 was gently laid on top of the pad. Samples were imaged as described in section "microscopy", followed by quantification (described in section "image analysis") to obtain the numbers of adsorbed phages and intracellular phage genomes for each cell.

Treatment with carbonyl cyanide m-chlorophenyl hydrazone (CCCP)

In experiments where the efficiency of phage entry in depolarized cells was examined (Figure 3H), cell washing and resuspension, phage dilution, and infection were performed using LBMM supplemented with 200 μM CCCP (similar concentration to that in Kralj et al.[58]). A no-treatment control was prepared using LBMM supplemented with 0.5% dimethylsulfoxide (DMSO). Following infection, the samples were diluted, mounted, and imaged as described above. This CCCP treatment was validated using propidium iodide (PI, resulting in the same degree of PI permeation as in infected cells, Figure S4C) and PROPS-expressing cells (resulting in a ~3× increase in PROPS fluorescence, Figure S5B).

Treatment with rifampicin

In experiments where the efficiency of phage entry in cells with inhibited transcription was examined (Figure S3D), we performed bulk infection using LBMM supplemented with 500 μg/mL rifampicin[42]; the negative control was prepared using LBMM supplemented with 1% DMSO. This rifampicin treatment was validated by following the OD_{600} of infected cultures (Figure S3C). Briefly, replication-competent phages (λ *cI857 stf*::P1*parS-kan*^{R}, at a ratio to bacteria of approx. 1) and 500 μg/mL rifampicin were added to exponentially-growing cells (MG1655, in LBMM) in a clear 48-well flat-bottom microplate (COSTAR). Incubation at 37°C with shaking (orbital mode, 1 mm amplitude) and OD_{600} measurement were performed using a TECAN M Nano plate reader. We found that 500 μg/mL rifampicin repressed all cell growth and viral development (Figure S3C).

Please cite this article in press as: Nguyen et al., Coinfecting phages impede each other's entry into the cell, Current Biology (2024), https://doi.org/10.1016/j.cub.2024.05.032

Data analysis

We used the model described in section "stochastic model of phage entry kinetics" below (see Table S5 for variable definitions) to capture the sublinear relation between the numbers of intracellular and adsorbed phages following bulk infection in LBMM. To do so, we used the parameters (η_n, k_n, τ_n) calibrated using the microfluidic assay in LBMM (section "measuring the kinetics of phage entries in the microfluidic device") and Equation 24 to calculate $\langle\lambda(n,t)\rangle$. To account for the additional time of sample dilution and mounting before the microscopy images were taken, we scanned for t between 5 and 12 minutes at a 0.1-minute increment. At each time point, the root-mean-squared-error (RMSE) between the model prediction and the data was calculated. The time at which RMSE was minimized was 9.1 minutes (Figure S2G).

This model prediction was possible because the kinetic parameters were already inferred from microfluidic infection data in LBMM. When kinetic parameters were not available (e.g., in other infection media surveyed in Figure S6), we used the following phenomenological expression to capture the average number of intracellular phage genomes:

$$\langle\lambda(n)\rangle = \frac{a\cdot n}{K+n}. \quad \text{(Equation 1)}$$

Equation 1 shares the same form with the Michaelis-Menten function, which is also a Hill function with a coefficient of 1. The fitted parameter values for each infection medium are given in the caption of Figure S6.

To capture the asymptotic value of entry efficiency in cells adsorbed by many phages (Figures 3H, 7B, and S1D), we used the following expression:

$$\langle\lambda/n\rangle = a\cdot e^{-b(n-1)} + c, \quad \text{(Equation 2)}$$

which describes an exponential decay with a baseline. This expression provides the entry efficiency in cells adsorbed by one phage ($= a + c$ when $n = 1$) and in cells adsorbed by many phages ($= c$ when $n \to \infty$).

To capture the distribution of intracellular phage numbers (e.g., Figure 5B), we used the following expression:

$$P(\lambda) = \left(\sum_{j=0}^{n} \frac{\mu^j e^{-\mu}}{j!}\right)^{-1} \frac{\mu^\lambda e^{-\mu}}{\lambda!}. \quad \text{(Equation 3)}$$

Equation 3 describes a truncated Poisson distribution for the random variable λ, controlled by a parameter μ. Truncation is necessary because there cannot be more intracellular phage genomes (λ) than the number of adsorbed phages (n).

We confirmed that Equations 1, 2, and 3 capture the corresponding predictions by the stochastic model (section "stochastic model of phage entry kinetics") over the experimentally relevant range of MOI and time.

Fitting procedure

Fitting to single-cell data was performed with bootstrapping (1000 iterations). In each iteration, a bootstrapped sample with the same number of cells as the original dataset was randomly drawn with replacement (implemented using the MATLAB 'datasample' function). Fitting to each bootstrapped sample was implemented with the MATLAB 'fit' function, using nonlinear least-squares optimization and the trust-region algorithm. Estimates and SE of the parameters were calculated from the mean and standard deviation (SD) of the fitted parameters' sampling distributions.

Measuring the efficiency of phage entry using SYTOX Orange

Infection and imaging

This assay was used to measure the entry efficiency of phage lambda (Figure S1D), T5, and P1 (Figure 7). MG1655 cells were grown and concentrated in ice-cold media as described in section "measuring the numbers of adsorbed phages and intracellular phage genomes following bulk infection". The resuspension media for lambda infection were LBMM and SM; the resuspension media for T5 and P1 infection were LB and SM, both supplemented with 1 mM or 5 mM $CaCl_2$, respectively for each phage.[62,85] Phage solutions were stained with SYTOX Orange and dialyzed into the corresponding solution as described in section "phage preparation". For each phage and each infection medium, an infection mixture at a phage-to-bacteria ratio of approx. 3 was prepared. The sample was incubated at 4°C for 30 minutes to allow for phage adsorption, diluted 1:10 in the pre-infection medium, immediately mounted on an agarose pad as described in section "measuring the numbers of adsorbed phages and intracellular phage genomes following bulk infection", and imaged as described in section "microscopy".

In contrast to the protocol in section "measuring the numbers of adsorbed phages and intracellular phage genomes following bulk infection", here, there was no 5-minute incubation at 35°C to trigger phage ejection before imaging. Instead, the enclosure in which the microscope was housed (see section "microscopy" for details) was set to 37°C, and phage entry took place on the agarose pad during imaging. Image acquisition was performed twice: Immediately after the sample was mounted onto the microscope (0 minutes), and after 10 minutes of incubation at 37°C. Quantification was performed as described in section "image analysis" to obtain the number of encapsidated phage DNA (using the SYTOX Orange signal) on each cell at 0 and 10 minutes.

Data analysis

The number of SYTOX Orange spots on the cell at 0 minutes was taken as the number of phages adsorbed to the cell. An entry event was defined to have occurred for every SYTOX Orange spot at 0 minutes that no longer exists at 10 minutes, interpreted as ejection of encapsidated phage DNA (Figures 7A and S1D). The efficiency of phage entry was calculated as the ratio of the number of entry

events and the number of adsorbed phages in the same cell. In Figures 7B and S1D, the efficiency of phage entry was used to fit Equation 2, describing an exponential decay with a baseline.

Measuring phage-induced membrane permeabilization using propidium iodide

Infection, staining, and imaging

MG1655 cells or MG1655 cells harboring pALA3047 (expressing CFP-ParB) were grown in LBMM supplemented with IPTG, and concentrated in either LBMM or SM as described in section "measuring the numbers of adsorbed phages and intracellular phage genomes following bulk infection". An infection mixture, using λ_{TY11} with fluorescently labeled capsids, was prepared at a phage-to-bacteria ratio of approx. 3, incubated for 30 minutes at 4°C for phage adsorption, then shifted to 37°C to trigger phage ejection. At each time point (5, 20, 35, and 50 min) during the incubation at 37°C, an aliquot of the infection mixture was taken, diluted 1:10, and mixed with propidium iodide (PI, final concentration 10 μM, following Cohen et al.[87]). The sample was incubated in the dark at RT for 5 minutes, then mounted and imaged as described in section "microscopy". Quantification was performed as described in section "image analysis" to obtain the number of adsorbed phages, the number of intracellular phage genomes, and the intracellular PI fluorescence of each cell.

Controls

Because PI was previously reported to perturb productive phage infection,[46] here, we only added PI to an aliquot of the infection mixture before imaging, while phage adsorption and entry both took place in the absence of PI. As a result, phage entry was not perturbed by PI. Indeed, the efficiency of phage entry in PI-stained samples was similar to that in the unstained sample (both in LBMM), and the sublinear relation between the numbers of intracellular and adsorbed phages was reproduced (Figure S4B).

For the negative control, cells that had gone through the same centrifugation and washing protocol as the infected sample were mixed with blank medium, incubated at 4°C for 30 minutes, and shifted to 37°C for 60 minutes (longer than the last time point of the infected sample). The sample was then stained with PI and imaged. The PI fluorescence in this uninfected control was similar to that in cells with no adsorbed phages in the infected sample (Figure S4C).

For the positive control, cells were permeabilized by incubation with 70% ethanol at RT for 30 minutes,[88] then washed and resuspended in PBS. Permeabilized cells were stained with PI and imaged. The PI fluorescence in ethanol-treated cells was approx. 50× higher than that in cells adsorbed by ~10 phages (Figure S4C). This suggested that the PI permeation observed in the infected sample did not reflect cell death (in contrast to, e.g., Yang et al.[89]). In addition, since the phage strain used in this experiment, λ_{TY11}, is incapable of the lytic pathway,[8,90] permeation of PI into the cell, even at 50 minutes after infection, was not due to the onset of cell lysis (in contrast to, e.g., Cohen et al.[87]).

PI was also used to validate our CCCP treatment protocol (section "measuring the numbers of adsorbed phages and intracellular phage genomes following bulk infection"). Briefly, cells were washed and resuspended in the medium supplemented with 200 μM CCCP, stained with PI, and imaged. The PI fluorescence in CCCP-treated cells was in the range of that in cells adsorbed by 1–10 phages, suggesting that our CCCP protocol can be used to emulate the perturbations caused by phage adsorptions (Figure S4C).

Data analysis

We fitted a linear equation to the intracellular PI fluorescence (F) as a function of the number of adsorbed phages (n):

$$F(n) = a \cdot n + b. \quad \text{(Equation 4)}$$

Here, the slope a provides an estimate for the degree of membrane permeabilization per infecting phage. Equation 4 was fitted to data at each time point (5, 20, 35, and 50 minutes), with bootstrapping as described above. The data and linear fits for LBMM are shown in Figures 3B, 4B, and S4D; the values of the slope a in LBMM at different times are shown in Figure 3C. The data and linear fit for SM are shown in Figure 4B. The inferred values of $F(n = 1)$ for both LBMM and SM are shown in Figure 4C.

A similar fitting procedure was performed for the intracellular PI fluorescence as a function of the number of intracellular phage genomes, $F(\lambda)$, shown in Figure S4D for infection in LBMM.

For infection in LBMM, calculations of the Pearson correlation coefficients between the PI fluorescence and the number of adsorbed phages, and between the PI fluorescence and the number of intracellular phage genomes were performed with bootstrapping (1000 iterations, implemented using the MATLAB 'corrcoef' function). We found that the PI fluorescence was positively correlated with the number of adsorbed phages and was not correlated with the number of intracellular phage genomes (Figure S4E).

We fitted the following expression to the efficiency of phage entry in LBMM as a function of the PI fluorescence:

$$\langle \lambda / n \rangle = a \cdot e^{-bF} + c. \quad \text{(Equation 5)}$$

Equation 5 provides an estimate of the entry efficiency in non-permeabilized cells ($= a + c$ when $F = 0$) and the asymptotic value in highly permeabilized cells ($= c$ when $F \to \infty$). Equation 5 was fitted to the pooled LBMM data from 5 and 20 minutes with bootstrapping as described above. Fitting results are shown in Figure 3D, and the fitted parameters are $a = 0.45 \pm 0.05$, $b = 0.004 \pm 0.002$, and $c = 0.26 \pm 0.08$.

Causal inference

Because the number of adsorbed phages is negatively correlated with the efficiency of phage entry (Figure 1C) and positively correlated with the intracellular PI fluorescence (Figure 3B), the observed correlation between the entry efficiency and the PI fluorescence

Please cite this article in press as: Nguyen et al., Coinfecting phages impede each other's entry into the cell, Current Biology (2024), https://doi.org/10.1016/j.cub.2024.05.032

(Figure 3D) could be due to the confounding effect of the number of adsorbed phages per cell. To control for this variable, we followed Kar et al.[56] and calculated the conditional correlation, r, between entry efficiency and PI fluorescence when the effect of the number of adsorbed phages is removed.

Using the pooled data from 5 and 20 minutes, we performed linear regressions of entry efficiency on the number of adsorbed phages, and of PI fluorescence on the number of adsorbed phages (Figure S4F). Cells with no adsorbed phages, in which the efficiency of phage entry is undefined, were not included in this analysis. The residuals following linear regressions represent variations in the entry efficiency and in the PI fluorescence due to sources other than the number of adsorbed phages. These residuals were denoted as Entry efficiency (Residual) and PI fluorescence (Residual) (Figures 3E and S4F) If there is no causal link between PI fluorescence and entry efficiency, the correlation between these residuals will be zero. However, we found that the Pearson correlation coefficient between Entry efficiency (Residual) and PI fluorescence (Residual), denoted as r(Entry efficiency, PI fluorescence|Number of adsorbed phages), is negative (Figure 3E). Calculation of correlation was performed with bootstrapping (1000 iterations), yielding $r = -0.27 \pm 0.04$. Performing the Student's t-test, we found that this negative correlation is statistically significant ($p-\text{value} \approx 3 \times 10^{-6}$). Therefore, compromise to membrane integrity was inferred to be a cause of impeded phage entry.

Measuring the time of the first phage entry following bulk infection

Infection, fixation, and imaging

MG1655 cells harboring pALA3047 (expressing CFP-ParB) were grown and concentrated as described in section "measuring the numbers of adsorbed phages and intracellular phage genomes following bulk infection". An infection mixture was prepared at a phage-to-bacteria ratio of approx. 0.5 and incubated at 4°C for 30 minutes. To trigger phage ejection and to prevent additional adsorptions, the infection mixture was diluted 1:1000 into prewarmed LBGM supplemented with IPTG in a baffled Erlenmeyer flask. The diluted infection mixture was shaken at 220 rpm in a 37°C water bath for 10 minutes, during which samples were extracted for fixation. A negative control (cells and blank solution) was also prepared and extracted at the end of the experiment.

Chemical fixation was performed as described in Yao et al.[8] Briefly, at each time point (immediately before the dilution to 37°C, then at 1, 2, 3, 4, 5, and 10 minutes), samples were aliquoted and mixed with formaldehyde (final concentration 3.7%) in PBS (final concentration 1×) for 30 minutes at RT. The samples were washed twice and concentrated in PBS, mounted as in Skinner et al.,[88] and imaged as described in section "microscopy". Quantification was performed as described in section "image analysis" to obtain the number of intracellular phage genomes in each cell.

Data analysis

At this phage-to-bacteria ratio (≈ 0.5), we assumed that all cells in the infection mixture were adsorbed by either 0 or 1 phage.[68] Hence, measurements obtained from the infected cells reflected the kinetics of phage entry in cells adsorbed by one phage. We fitted the following expression to the time-dependent average number of intracellular phage genomes:

$$\langle \lambda(t) \rangle = a\left(1 - e^{-k(t-\tau)}\right) \text{ for } t \geq \tau, \text{and 0 otherwise.} \quad \text{(Equation 6)}$$

Equation 6 was derived from Equation 37 in section "stochastic model of phage entry kinetics" below. Here, the parameter a describes the fraction of cells with intracellular phage genomes among all cells in the infection mixture, thus representing both the entry (η) and adsorption efficiencies. Fitting was performed with bootstrapping as described above. Both the data and the fit in Figure S1I are shown after rescaling, i.e., $^1/_a \cdot \langle \lambda(t) \rangle$ vs. t. The measured kinetics from this bulk assay is compared with that in the microfluidic assay and the literature in Figure S1G.

Measuring the kinetics of phage entries in the microfluidic device

Preparation of cells and phages

Cultures of MG1655 harboring p2973 or pALA3047 were grown at 37°C in LBMM supplemented with IPTG and 100 μg/mL ampicillin as described in section "bacterial growth conditions". Upon reaching $OD_{600} \approx 0.3$–0.4, the culture was diluted 5× in LBMM supplemented with IPTG, and introduced into the microfluidic device as described below. The purified phage stock (λ_{TY11} with fluorescently labeled capsids, described in section "phage preparation") was diluted to approx. 2×10^{10} PFU/mL using LBMM supplemented with IPTG. In this assay, gpD-mTurquoise2 or gpD-EYFP phages were used to infect MG1655 harboring p2973 or pALA3047 (expressing mCherry-ParB or CFP-ParB), respectively.

Setting up and operating the microfluidic device

Microfluidic experiments were performed in B04A plates of the CellASIC ONIX or ONIX2 microfluidics system (MilliporeSigma), controlled using the ONIX FG software. The microfluidic system was incubated in a temperature-controlled enclosure (Okolab), set at 37°C. Cells, phages, and blank medium (LBMM supplemented with IPTG) were pipetted into inlets of a microfluidic plate (pre-purged as described in the instruction manual). The observation chamber was first primed with the blank medium. Cells were then loaded into the chamber and grown for 30 minutes (approx. one generation). Fresh medium was constantly exchanged during this time using a flow pressure of 1 psi. To begin infection, phages were perfused into the chamber at 10 psi for 2 minutes, followed by the blank medium at 10 psi for 4 minutes to wash out excess phages. Constant medium exchange at 1 psi was resumed until the end of the experiment. Image acquisition was performed throughout this perfusion protocol (described in section

Please cite this article in press as: Nguyen et al., Coinfecting phages impede each other's entry into the cell, Current Biology (2024), https://doi.org/10.1016/j.cub.2024.05.032

"microscopy"). Quantification was performed as described in section "image analysis" to obtain the numbers of adsorbed phages and intracellular phage genomes for each cell at every time point. The time series of phage adsorptions and entries from a representative experiment are shown in Figure S2A.

Data analysis: Estimation of model parameters for MOI = 1

In the following analyses, the expressions used for model fitting are derived in section "stochastic model of phage entry kinetics", and the variables are defined in Table S5. Model fitting was implemented with the MATLAB 'lsqcurvefit' function, using nonlinear least-squares optimization and the trust-region algorithm. Fitting was performed with bootstrapping (1000 iterations for each single-cell dataset), as described above.

We first examined the entry kinetics in cells with one adsorbed phage (7 experiments acquired at 1-minute imaging frequency, each yielding 6–49 cells with $n = 1$). For each experiment, we calculated the time-dependent average number of intracellular phages in cells adsorbed by one phage, $\langle\lambda(n = 1,t)\rangle$, and fitted Equation 37 to this data. The inferred parameters are $\eta_1 = 0.56 \pm 0.04$, $k_1 = 0.011 \pm 0.004\ s^{-1}$, and $\tau_1 = 43.0 \pm 10.5$ s (mean and SE of the fitted parameters of the 7 experiments; the subscript "1" denotes parameters for $n = 1$). Using the pooled dataset from all 7 experiments yielded similar values: $\eta_1 = 0.56 \pm 0.04$, $k_1 = 0.010 \pm 0.001\ s^{-1}$, and $\tau_1 = 35.9 \pm 5.6$ s (SE from bootstrapping); this fitting result is shown in Figure 2C. The inset of Figure 2C shows $\log(1 - \langle\lambda\rangle/\eta)$ vs. $t - \tau$; the linearity of this graph supports the analytical expression in Equation 37. The inferred parameters are compared with those obtained in the bulk assay and the literature in Figures S1F–S1H.

We next used Equation 35 and the fitted parameters (η_1, k_1, τ_1) above to calculate the probability density of phage entry time, $f(T_1|n = 1)$. To compare with the experimental data (Figure 2D), we binned the predicted probability density by the imaging inter-frame interval (calculated using the MATLAB 'trapz' function):

$$P(T_1 = t|n = 1) = \int_{t-1}^{t} f(T_1 = t'|n = 1)\, dt'. \quad \text{(Equation 7)}$$

Estimation of model parameters for MOI > 1

Next, we assumed that the parameters fitted using cells with $n = 1$ were also applicable to cells with $n > 1$. Following this assumption (termed the MOI-independent model), we used Equation 24 and the parameters (η_1, k_1, τ_1) from above to predict the time-dependent average number of intracellular phage genomes in cells adsorbed by multiple phages, $\langle\lambda(n,t)\rangle$, and compared these predictions with the data for $n \in [2, 10]$ (beyond which the number of cells for a given number of adsorbed phages is less than 5). As n increases, the model prediction becomes poorer (Figures 2E and S2D). We concluded that the MOI-independent model was inappropriate, and the parameters for $n = 1$ cannot be applied to $n > 1$.

Instead, we allowed all three parameters of the model to vary with the number of adsorbed phages. To do so, we divided the pooled dataset into subsets of cells with different n, and fitted Equation 24 to each of these data subsets, yielding separate sets of parameters (η_n, k_n, τ_n) for each n value. This model (termed the MOI-dependent η, k, τ model), captured the time-dependent average number of intracellular phages well (Figure S2D). The average RMSE of the MOI-dependent η, k, τ model is 0.0862, a considerable improvement compared to the MOI-independent model with RMSE = 0.887 (Figure S2B). Examining how each parameter varies with n, we noted that both the fitted η_n and k_n appeared to decrease with n, whereas τ_n showed no consistent trend (Figure S2C). We hypothesized that a dependence of η and k on the number of adsorbed phages (n) is necessary to capture the data, while τ can remain MOI-independent.

To test this hypothesis, we fitted a model in which only η and k were allowed to vary with n, while τ was constrained at τ_1, and obtained the parameters (η_n, k_n, τ_1) for each n value. Predictions by this model (termed the MOI-dependent η, k model) were indistinguishable from those of the MOI-dependent η, k, τ model (Figure S2D). The average RMSE of the MOI-dependent η, k model (= 0.0825) is similar to that of the MOI-dependent η, k, τ model (Figure S2B). When we investigated the other 5 models in which one or two of the parameters were allowed to vary with the number of adsorbed phages, none of them achieved a lower RMSE than when only η and k were allowed to vary (Figure S2B). Therefore, we concluded that the MOI-dependent η, k model is the most appropriate one to describe the observed data.

Parametrization of the MOI-dependent model

To describe the overall behaviors of η and k as a function of n, and to infer parameter values when data of a given n was not available, we parametrized η_n and k_n as exponentially decaying functions of n:

$$\eta_n = a_\eta \cdot e^{-b_\eta(n-1)} + c_\eta, \quad \text{(Equation 8)}$$

$$k_n = a_k \cdot e^{-b_k(n-1)} + c_k. \quad \text{(Equation 9)}$$

The fitted values of η and k from the MOI-dependent η, k model above were used to fit Equations 8 and 9, respectively. Fitting was weighted by the natural logarithm of the number of cells with a given n. The results of this parametrization are shown in Figure 2F. For η, $a_\eta = 0.458$, $b_\eta = 0.0762$, and $c_\eta = 0.131$. For k (unit, s^{-1}), $a_k = 0.00450$, $b_k = 0.456$, and $c_k = 0.00479$. As for τ, we simply set $\tau_n = \tau_1 = 35.9 \pm 5.6$ s. This set of inferred parameters (η_n, k_n, τ_n) constitutes the MOI-dependent model of entry dynamics.

Please cite this article in press as: Nguyen et al., Coinfecting phages impede each other's entry into the cell, Current Biology (2024), https://doi.org/10.1016/j.cub.2024.05.032

To predict the distribution of intracellular phage numbers at a given time, we used Equation 33 and these inferred parameters (η_n, k_n, τ_n) to calculate $P(\lambda|n,t)$. These predictions are shown in Figures 2G and S2E for $t \in [0, 10]$ min and $n \in [2, 4]$ (beyond which the sample size is smaller than 30 cells).

We also used the inferred parameters to predict the relation between the numbers of adsorbed and intracellular phages at different times. This was calculated using Equation 24 and plotted as $\langle\lambda(n)\rangle$ separately for each time point $t \in [0, 10]$ min (Figures 2H and S2F). Using the same model parameters, we also captured the values observed in bulk infection assays (Figure S2G, described above in section "measuring the numbers of adsorbed phages and intracellular phage genomes following bulk infection").

Validating the ParB-*parS* labeling system using SYTOX Orange

Experimental protocol

To measure the detection efficiency of the ParB-*parS* system (Figure S1C), we used SYTOX Orange to stain the DNA of phages whose capsids are labeled with gpD-EYFP (produced as described in section "phage preparation"), and infected cells expressing CFP-ParB. Infection was performed as described in section "measuring the kinetics of phage entries in the microfluidic device". Imaging was performed at the end of the experiment (described in section "microscopy"), followed by quantification as described in section "image analysis" to obtain the numbers of adsorbed phage capsids, encapsidated phage DNA, and intracellular phage genomes in individual cells.

Data analysis

An entry event was defined to have occurred for every phage capsid without encapsidated DNA (i.e., gpD-EYFP foci without SYTOX Orange signal). If the ParB-*parS* system faithfully detects intracellular phage genomes, there will be a ParB-*parS* spot for every corresponding entry event. In other words, we predicted the following relation:

$$N_{\mathrm{ParB-parS}} = N_{\text{fluorescent capsids}} - N_{\text{SYTOX Orange}}, \quad \text{(Equation 10)}$$

in which N_i is the number of fluorescent spots of type i in each cell. The fitted slope of $N_{\mathrm{ParB-parS}}$ vs. $N_{\text{fluorescent capsids}} - N_{\text{SYTOX Orange}}$ is 0.89 ± 0.04 (Figure S1C, SE from bootstrapping as described above).

Correcting for the efficiency of SYTOX Orange labeling

If SYTOX Orange fails to stain the encapsidated phage DNA, the capsid would appear to be empty regardless of whether ejection has occurred. As a result, an entry event would be falsely registered, and the detection efficiency of ParB-*parS* would be underestimated.

To correct this underestimation, we performed a simple stochastic simulation as follows. For each cell, given $N_{\text{fluorescent capsids}}$, we generated a random number from the following binomial distribution (implemented using the MATLAB 'binornd' function):

$$N_{\text{stained particles}} \sim \mathrm{Binom}\left(N_{\text{fluorescent capsids}}, \eta_{\text{SYTOX Orange}}\right), \quad \text{(Equation 11)}$$

in which $\eta_{\text{SYTOX Orange}}$ is the labeling efficiency of SYTOX Orange (91.9% ± 1.6%, measured as described in section "phage preparation"). For each cell, $N_{\text{stained particles}}$ simulates the number of phage particles that were stained with SYTOX Orange prior to infection. This simulation was performed for all cells in the original dataset, yielding a simulated dataset of the same size. The fitted slope of $N_{\mathrm{ParB-parS}}$ vs. $N_{\text{stained particles}} - N_{\text{SYTOX Orange}}$ provided a corrected estimate of the detection efficiency of the ParB-*parS* system. The distribution of this simulated slope value (n = 1000 realizations) is shown in the inset of Figure S1C. The mean and SD of this distribution is 0.93 ± 0.02, suggesting the detection efficiency of the ParB-*parS* system was approx. 93%.

Validating the CCCP treatment protocol using PROPS

Our protocol for carbonyl cyanide *m*-chlorophenyl hydrazone (CCCP) treatment (sections "measuring the numbers of adsorbed phages and intracellular phage genomes following bulk infection" and "optical trap assay") was validated using PROPS-expressing cells. Cultures of MG1655 pJMK001 were grown as described in section "bacterial growth conditions". Following PROPS induction, cells were washed and concentrated 5× in LBM supplemented with either 200 μM CCCP or 0.5% DMSO (serving as a negative control). Samples were mounted and imaged as described in section "microscopy", and the PROPS fluorescence was quantified as described in section "image analysis".

The PROPS fluorescence in cells depolarized using CCCP was approx. 3× higher than that in the DMSO control (Figure S5B). This fold-change is in agreement with Kralj et al.,[58] thus validating our protocol for CCCP treatment.

Microscopy

Equipment and setup

For all experiments except for those involving section "optical trap assay", either one of the following two inverted epifluorescence microscopes was used. The first one is an Eclipse T*i* (Nikon) system, equipped with a mercury lamp (Intensilight C-HGFIE, Nikon), a CMOS camera (Prime 95B, Photometrics), and a 100×, NA 1.45, oil-immersion phase-contrast objective lens (Plan Apo, Nikon). The second one is an Eclipse T*i*2 (Nikon) system equipped with an LED light source (X-Cite XYLIS); the camera and the objective lens were identical to the first setup. The microscopes were installed on a pneumatically-supported vibration-isolation table (CleanBench) and placed in a temperature-controlled enclosure (Okolab). Microscope operation and image acquisition were performed using the NIS-Elements software (Nikon). For phase contrast imaging, we used an exposure time of 100 ms. For fluorescence imaging, we used the filter sets listed in Table S4, with exposure times ranging between 50 ms and 400 ms.

Please cite this article in press as: Nguyen et al., Coinfecting phages impede each other's entry into the cell, Current Biology (2024), https://doi.org/10.1016/j.cub.2024.05.032

Snapshot imaging

Samples were mounted using coverslips and an agarose pad (e.g., as in section "measuring the numbers of adsorbed phages and intracellular phage genomes following bulk infection"), and placed on a universal specimen holder (Ti2-S-HU, Nikon). Images were acquired at multiple fields of view (*xy*-positions), located at least 300 μm apart to minimize photobleaching across fields of view. The different fields of view were located using motorized stage control. For each field of view, the phase contrast channel was imaged first, followed by the fluorescence channels. For each channel, images were taken at 7 focal planes (*z*-slices), with steps of 300 nm apart.

Time-lapse imaging

For imaging infection in the microfluidic device, CellASIC ONIX B04A plates were prepared as described in section "measuring the kinetics of phage entries in the microfluidic device" and placed on a well-plate holder (Ti2-S-HW, Nikon). The imaging frequency was either 1 minute (most experiments), 2 minutes, or 10 minutes (pilot or control experiments). For each time point, all of the fields of view were imaged. For each field of view, all of the phase contrast and fluorescence channels were imaged. For each channel, images were taken at 3 focal planes, with steps of 400 nm apart. Image acquisition was initiated at least 1 minute before phage perfusion and terminated no earlier than 20 minutes afterwards.

For imaging infection on agarose pads (section "measuring the efficiency of phage entry using SYTOX Orange"), the setup was similar to that for snapshot imaging. Image acquisition was performed twice, at 0 minutes (immediately after the sample was mounted) and 10 minutes (after incubation at 37°C).

Image analysis

Analysis was performed on the original images (before contrast adjustment was performed to produce representative images, described below), using Nikon NIS-Elements, ImageJ2/Fiji,[82] and MATLAB. In all analyses, the phase contrast channel provides information regarding the outline, size, and morphology of bacterial cells.

Measuring single-cell MOI

To quantify the numbers of extracellular phages (using DAPI, gpD-mTurquoise2, gpD-EYFP, or SYTOX Orange) and intracellular phage genomes (using CFP-ParB or mCherry-ParB), we manually counted the number of diffraction-limited fluorescent foci (spots) on the cell surface or inside the cell, respectively, in the corresponding fluorescence channels.

In time-lapse assays using the microfluidic device, for each cell tracked over the course of the experiment, the numbers of adsorbed phages and of intracellular phage genomes were recorded at each time point. Using this time series with respect to the beginning of phage perfusion, the times of phage adsorptions and entries were inferred. For example, if the numbers of adsorbed phages at (0, 1, 2, 3, 4,…) minutes were (0, 0, 1, 3, 3,…), the 1st adsorption event was considered to have occurred between 1 and 2 minutes, while the 2nd and 3rd adsorptions both took place between 2 and 3 minutes. Only cells with synchronized phage adsorptions—defined to be those with the first and last adsorption events within 2 minutes of one another—were used for model fitting. For each cell, the average time at which phages adsorbed to the cell was calculated. The time-dependent numbers of intracellular phage genomes and the entry times of individual phages were calculated with respect to this cell-specific average adsorption time (i.e., time since phage adsorption, set to be $t = 0$).

Measuring propidium iodide (PI) fluorescence

Using phase contrast, we performed manual segmentation to identify a region of interest (ROI) corresponding to each cell and measured the average fluorescence of PI (in arbitrary units, A.U., per pixel) within the ROI. Because some of the phage particles exhibited PI signal (corresponding to the encapsidated DNA), the intracellular fluorescence was measured using the focal plane at which such foci were not visible. The PI fluorescence of each cell was corrected for the average background outside the cells in the same field of view, then normalized by a factor equal to 1/1000 of the fluorescence in ethanol-treated cells (section "measuring phage-induced membrane permeabilization using propidium iodide"). Cells with overwhelming PI fluorescence (< 0.5% of the dataset, comparable to that in ethanol-treated cells) were excluded from the analysis.

Measuring PROPS fluorescence

PROPS fluorescence in individual cells was quantified using ROI in the same manner as PI, as described above. PROPS fluorescence was corrected for the background outside the cell in the same field of view, then normalized using the average intensity of cells in the negative control. Hence, the PROPS fluorescence following CCCP treatment or phage infection was reported in fold-change, as in Kralj et al.[58]

Optical trap assay

Preparation of cells and phages

For this assay, we followed the protocol from Min et al.[59] Briefly, cultures of MG1655 or MG1655 harboring pJMK001 (expressing PROPS) were grown as described in section "bacterial growth conditions". Cells were centrifuged at 1300×g for 10 minutes at RT, resuspended in the same volume in the motility buffer (MB), and diluted 5× in the trap motility buffer (TMB) or TMB supplemented with 10 mM $MgSO_4$ (TMBM) as specified below (see Table S3 for the composition of these buffers). When required, phages were stained with SYTOX Orange as described in section "phage preparation".

Setup of the optical traps and the flow chamber

All trap-related experiments were performed at room temperature. The optical traps and epifluorescence setup were described in Mears et al.[91] The three-channel flow chamber (Figure 3F) was made as described in Min et al.[59] Solutions were perfused at a

Please cite this article in press as: Nguyen et al., Coinfecting phages impede each other's entry into the cell, Current Biology (2024), https://doi.org/10.1016/j.cub.2024.05.032

flow rate of 0.33 μL/min, resulting in a linear speed of 35 μm/s. The cell positions in the optical trap were recorded at a rate of 666 Hz, and the fluorescence of SYTOX Orange or PROPS was imaged at a rate of 10 Hz, using a 532 nm excitation laser.

Measuring the membrane potential following CCCP treatment

In this experiment, the three channels of the flow chamber contained (i) PROPS-expressing cells in TMB, (ii) blank TMB, and (iii) TMB supplemented with 200 μM CCCP. Individual cells were first trapped from the cell channel, then moved into the blank channel. Each cell was kept in the blank channel for approx. 1 minute to record the basal flagellar rotation frequency, then moved into the CCCP channel, where the loss of motility and the increase in PROPS fluorescence were observed within ~5 seconds (Figure S5C).

Measuring the membrane potential following phage adsorption

In this experiment, the three channels of the flow chamber contained (i) cells in TMBM, (ii) blank TMBM, and (iii) phages at approx. 1×10^{10} PFU/mL in TMBM. Two combinations of phages and cells were used: (i) Phages stained with SYTOX Orange, infecting MG1655 cells (Figures 3F and 3G); and (ii) Unstained phages, infecting PROPS-expressing cells (Figures S5D and S5E).

Individual cells were first trapped from the cell channel, then moved into the blank channel for approx. 1 minute to record the basal flagellar rotation frequency. Each cell was then moved into the phage channel for at least 5 minutes. During this time, if a phage (visualized using SYTOX Orange) stably adsorbed to the cell, the cell was considered to be infected and was moved back into the blank channel. Cells with no adsorbed phage were used as a negative control. Cells were monitored in the blank channel for at least 30 minutes or until motility was lost. In this experiment, $t = 0$ was defined to be the time the phage adsorbed to the cell, or when a cell with no adsorbed phage was moved back into the blank channel.

In experiments with PROPS-expressing cells, cells were kept in the phage channel for at least 30 minutes or until motility was lost. In this case, $t = 0$ was defined to be the time the cell was moved into the phage channel. Because phages were not stained in this experiment, the adsorption time and the number of adsorbed phages could not be measured.

Data analysis

To extract the flagellar rotation frequency, the cell position in the traps was analyzed using wavelet analysis as described in Min et al.[60] A typical cell in this assay had a flagellar rotation frequency of approx. 100 Hz. A cell was determined to have lost motility, indicating membrane depolarization, when the wavelet amplitude of the flagellar rotation peak decreased below a threshold (set manually).

Figure 3G shows a "survival curve" for the fraction of motile cells over time following phage adsorption, $f_{\text{motile}}(t)$. Data within the first 10 minutes was used to fit the following expression:

$$f_{\text{motile}}(t) = e^{-\kappa t}. \quad \text{(Equation 12)}$$

To estimate κ, fitting of Equation 12 to data was performed with bootstrapping as described above. The fitting result is shown in Figure 3G, with $\kappa = 0.12 \pm 0.06\ \text{min}^{-1}$.

In experiments involving PROPS, the PROPS fluorescence was corrected for the background fluorescence, then normalized using the basal fluorescence prior to CCCP treatment or phage adsorption (Figure S5E; see also, section "image analysis"). Hence, the PROPS fluorescence was reported in fold-change, as in Kralj et al.[58]

Preparation of representative images

To prepare representative images (Figures 1A, 2A, 3A, 3F, 7A, S1A, S1B, S1D, S4A, and S5B), we used Nikon NIS-Elements and ImageJ2/Fiji to first perform a maximum intensity projection across the focal planes. Then, to remove background and non-specific fluorescence, we applied contrast adjustments to the entire image and to all samples. Pseudo-coloring of the fluorescence channels was then performed. Extracellular phage capsids (gpD-mTurquoise2 or gpD-EYFP) were pseudo-colored in cyan, and intracellular phage genomes (mCherry-ParB or CFP-ParB) were pseudo-colored in red. DAPI, SYTOX Orange, propidium iodide (PI), and PROPS were shown in other colors. When appropriate, the relevant channels were combined into a single image, and cropped to highlight the cell or area of interest. Scale bars were provided for all images (80 nm per pixel for images obtained with the optical traps, and 44 nm per pixel otherwise).

Potassium efflux assay

For this assay, we followed the protocols from Kronheim et al.[46] and Leavitt et al.[92] Cultures of MG1655 were grown at 37°C in LBMM as described in section "bacterial growth conditions". When the culture reached $OD_{600} \approx 0.3$–0.4, cells were centrifuged, washed once in SM3 buffer (described in Kronheim et al.[46]), and resuspended in SM3 at the original concentration. The cell suspension was incubated at 37°C for at least 5 minutes before infection was performed. The purified phage stock (section "phage preparation"), diluted to 1×10^{10} PFU/mL in SM3, was added to the cells at a phage-to-bacteria ratio of approx. 100. For the negative control, the same volume of blank SM3 buffer was added to the cell suspension. The concentration of K^+ ions in the medium was measured using an Orion K^+ ISE Electrode (ThermoScientific) and a FiveEasy pH/mV meter (Mettler Toledo). The voltage readings were manually recorded once every 10 seconds from 5 minutes before phage addition (the baseline) to 15 minutes after. Voltage readings were converted to molarity using a calibration curve, obtained using K^+ standard solutions as prescribed by the electrode's instruction manual. The total K^+ content in the cells was determined by treating the same amount of cells with the BugBuster 10× Reagent (Millipore), followed by incubation at 95°C–100°C for 5 minutes to lyse the cells. This total value was used for normalization to calculate the time-dependent fraction of K^+ released due to phage infection (Figure S5A).

Please cite this article in press as: Nguyen et al., Coinfecting phages impede each other's entry into the cell, Current Biology (2024), https://doi.org/10.1016/j.cub.2024.05.032

Measuring the frequency of lysogeny following infection in different media

Infection and selection

This assay was an adaptation of Yao et al.,[8] but instead of using agar plates, we used a plate reader to count the number of lysogens.[66] MG1655 cells, grown as described in section "bacterial growth conditions", were centrifuged, washed in LBM or SM, and concentrated 20× in LBM or SM (similarly to section "measuring the numbers of adsorbed phages and intracellular phage genomes following bulk infection"). Two 2.5× dilution series of the phage stock (produced as described in section "phage preparation") were prepared in LBM or SM (from $\sim 7.5\times10^{7}$ to $\sim 1.2\times10^{11}$ PFU/mL). Two infection series in LBM and SM (phage-to-bacteria ratio ranging from ~0.05 to ~50) were prepared, incubated at 4°C for 30 minutes, and shifted to 35°C for 5 minutes. Then, 2 μL of each infection mixture was diluted into duplicate wells containing 500 μL LBM, in a clear 48-well flat-bottom microplate (COSTAR). Samples were incubated for 1 hour at 30°C with shaking (orbital mode, 1 mm amplitude) in a TECAN F200 Pro plate reader to allow the lysogenic cells to express kanamycin resistance. Each culture was then supplemented with 50 μg/mL kanamycin, and incubation with shaking was resumed. For each infection series, an uninfected control without kanamycin selection was also prepared. The plate reader was set to measure the optical density (OD) of the cultures once every 5 minutes for ~24 hours.

Our SM infection procedure is different from protocols involving pre-infection starvation (Table S6), which were reported to result in a higher frequency of lysogeny.[5,68,93,94] In these studies, starvation prior to infection was achieved by either growing cells into stationary phase[68,94] or by incubating exponentially growing cells in a solution without nutrients for at least one generation (in one case with shaking at 37°C[93]) before adding phages.[5] Here, we resuspended exponentially growing cells in cold SM buffer and immediately added phages to begin adsorption. Thus, our cells were not starved before infection, and the observed lower frequency of lysogeny following infection in SM (analyzed as described below) does not contradict previous studies.

We also note that in Kourilsky,[5] after starved cells had been incubated with phages in a 10 mM $MgSO_4$ solution for 30 minutes at 4°C, the infection mixture was diluted into tryptone-maltose broth at 32°C to trigger phage ejection. Our survey of different entry media (Figure S6) showed that in solutions containing tryptone and/or maltose, the average number of intracellular phage genomes does not saturate at one (as in SM, used in this study). Thus, the high frequency of lysogeny found in Kourilsky[5] was conceivably due to the combined effect of starvation and a medium permissive of multiple phage entries.

Data analysis: Calculating the frequency of lysogeny

Under kanamycin selection, only lysogenic cells, which harbor prophages with the resistance cassette, can grow.[6,8,66,68] As a result, the OD curves of infected cultures can be used to infer the number of lysogens. The frequency of lysogeny, f_{lysogeny}, is defined to be the fraction of lysogenic cells (L_0) among total cells (T_0), calculated as follows:

$$f_{\text{lysogeny}} = \frac{L_0}{T_0} = 2^{-\frac{1}{g}\left(t_L^* - t_T^*\right)} = 2^{-\frac{\Delta t^*}{g}}. \qquad \text{(Equation 13)}$$

Here, g is the doubling time of the cell cultures (approx. 35 min). t_L^* and t_T^* are the times the infected culture under selection and the uninfected culture without selection, respectively, reached a threshold OD (= 0.1) during the exponential growth phase. Hence, $\Delta t^*/g$ is the difference in the number of elapsed generations between the two samples (Figure S7B).

Following this calculation, the maximum frequencies of lysogeny observed under the two conditions are $f_{\text{max,LBM}} = 0.012 \pm 0.003$ and $f_{\text{max,SM}} = 0.0004 \pm 0.0002$ (Error bars indicate SE from $n = 2$ replicates and variation in the parameter g). Our model in section "modeling bulk lysogenization following phage entry in different media" aimed to use the medium-specific entry dynamics to account for this difference ($f_{\text{max,LBM}}/f_{\text{max,SM}} \approx 32.1$).

Model fitting

We fitted Equation 20 (derived in below) to the frequency of lysogeny as a function of the phage-to-bacteria ratio, $f_{\text{lysogeny}}(M)$, obtained following infection in LBM and SM. Only a and $q_{\max}$ were fitted parameters. Because the phage strain used in this assay was replication-deficient, following Kourilsky[5] and Yao et al.,[8] we set MOI* to be 3. Parametrization of $\mu_n = \langle\lambda(n)\rangle$ was also pre-determined using microscopy data (see Figure S6 for the parameters following infection in LBMM and SM).

While Equation 20 includes a summation from 0 to infinity for n, for numerical purposes, the sum was taken from 0 to either 4-fold of M or to 10, whichever is larger. Beyond this range, the probability $P(n > 4M)$ or $P(n > 10)$ becomes vanishingly small and was ignored. We confirmed that increasing the upper limit of this sum added computational time but resulted in no change in the fitted values.

Fitting was implemented with the MATLAB 'lsqcurvefit' function, using nonlinear least-squares optimization and the trust-region algorithm. Because the sample size was small (6 data points for each series in LBM or SM), we bootstrapped each series by fitting to all 6 data points, then fitting to two subsets of the data (the 1st, 3rd, 5th points, and the 2nd, 4th, and 6th points). Estimates and SE of the parameters were calculated from the mean and SD of these three fitting runs.

This fitting procedure yielded the parameters a and $q_{\max}$ specific for each medium. In LBM, $q_{\text{max,LBM}} = 0.0116 \pm 0.0009$, and in SM, $q_{\text{max,SM}} = 0.003 \pm 0.001$. We interpreted these fitting results as follows (Figure 5A). The experimentally observed $f_{\text{max,LBM}}/f_{\text{max,SM}} \approx 32.1$ was captured using an inferred ratio $q_{\text{max,LBM}}/q_{\text{max,SM}}$ of only 3.4. This suggests that the remaining 9.4-fold could be attributed to the other difference between the two media: the specific parametrization of the distribution of intracellular phage numbers, $P(\lambda|n)$.

Differences in the fitted parameter a ($a_{\text{LBM}} = 0.59 \pm 0.05$, $a_{\text{SM}} = 0.20 \pm 0.05$) only shifted the lysogeny-vs.-MOI curves horizontally when plotted in log-log scale and did not contribute to the maximum frequency of lysogeny. Data and the fits in Figure 5A are shown with the phage-to-bacteria ratios rescaled, $f_{\text{lysogeny}}(a \cdot M)$, as done in Yao et al.[8]

Please cite this article in press as: Nguyen et al., Coinfecting phages impede each other's entry into the cell, Current Biology (2024), https://doi.org/10.1016/j.cub.2024.05.032

Modeling bulk lysogenization following phage entry in different media

Description of the model

Following Kourilsky,[5] Zeng et al.,[6] and Yao et al.[8] our model maps the phage-to-bacteria ratio in the infection mixture to a single-cell MOI, and the MOI to a probability at which the infected cell is lysogenized. However, while previous models omitted the entry stage, thus implicitly assuming all adsorbed phages enter the cell instantaneously, ours includes an explicit term for the entry dynamics. The model is depicted in Figure 5B.

The frequency of lysogeny as a function of the phage-to-bacteria ratio, $f_{\text{lysogeny}}(M)$, is described using the following function:

$$f_{\text{lysogeny}}(M) = \sum_{n=0}^{\infty}\left[P(n|M)\sum_{\lambda=0}^{n}P(\lambda|n)\cdot Q(\lambda)\right]. \quad \text{(Equation 14)}$$

Equation 14 consists of three terms. The first term, $P(n|M)$, is the probability a cell is adsorbed by n phages, given a phage-to-bacteria ratio M. Following Kourilsky[5] and Yao et al.[8] we assumed phage-bacteria collisions follow Poisson statistics. Hence, the number of adsorbed phages per cell follows the distribution below:

$$P(n|M) = \frac{(aM)^n e^{-aM}}{n!}, \quad \text{(Equation 15)}$$

in which a scaling factor a accounts for both the adsorption efficiency and the accuracy in measuring phage and cell concentrations.

In Equation 14, $P(\lambda|n)$ is the probability a cell has λ intracellular phage genomes, given n adsorbed phages. This distribution is described in the next subsection.

Finally, $Q(\lambda)$ is the probability a cell with λ intracellular phage genomes is lysogenized. Following Kourilsky[5] and Yao et al.[8] we assumed that coinfection by $\lambda \geq \text{MOI}^*$ phages is required for lysogeny. Accordingly, $Q(\lambda)$ is described using the following step-function:

$$Q(\lambda) = \begin{cases} 0 & \text{for } \lambda < \text{MOI}^* \\ q_{\max} & \text{for } \lambda \geq \text{MOI}^*, \end{cases} \quad \text{(Equation 16)}$$

in which $q_{\max}$ is the maximum probability of lysogenization.

Using this parametrization of $Q(\lambda)$, Equation 14 can be rewritten as follows:

$$f_{\text{lysogeny}}(M) = q_{\max}\sum_{n=0}^{\infty}\left[P(n|M)\sum_{\lambda=\text{MOI}^*}^{n}P(\lambda|n)\right]. \quad \text{(Equation 17)}$$

Parametrization of the distribution of intracellular phage numbers

If we assume that all adsorbed phages enter the cell instantaneously, $P(\lambda|n)$ can be parametrized as:

$$P(\lambda|n) = \begin{cases} 0 & \text{for } \lambda \neq n \\ 1 & \text{for } \lambda = n. \end{cases} \quad \text{(Equation 18)}$$

As a result, Equation 17 is rewritten as follows.

$$f_{\text{lysogeny}}(M) = q_{\max}\sum_{n=\text{MOI}^*}^{\infty}P(n|M) = q_{\max}\left(1 - \sum_{n=0}^{\text{MOI}^*-1}\frac{(aM)^n e^{-aM}}{n!}\right). \quad \text{(Equation 19)}$$

We note that Equation 19 has been reduced to the expression used to fit the bulk lysogenization data in Yao et al.[8]

To incorporate stochastic phage entry into the model, we parametrized $P(\lambda|n)$ using Equation 3: For cells adsorbed by n phages, the intracellular phage number λ is assumed to follow a truncated Poisson distribution controlled by a parameter μ_n. With this parametrization of $P(\lambda|n)$, Equation 17 is rewritten as follows:

$$f_{\text{lysogeny}}(M) = q_{\max}\sum_{n=0}^{\infty}\left[\frac{(aM)^n e^{-aM}}{n!}\left(\sum_{j=0}^{n}\frac{\mu_n^j e^{-\mu_n}}{j!}\right)^{-1}\sum_{\lambda=\text{MOI}^*}^{n}\frac{\mu_n^\lambda e^{-\mu_n}}{\lambda!}\right]. \quad \text{(Equation 20)}$$

For simplicity, we set μ_n, the mean of the Poisson distribution before truncation, to be equal to $\langle\lambda(n)\rangle$, the average number of intracellular phages in cells adsorbed by n phages. $\langle\lambda(n)\rangle$ is parametrized by Equation 1, using experimental data obtained in each infection media (Figure S6). Therefore, $P(\lambda|n)$ is also specific to each medium (e.g., Figure 5B).

The values of $f_{\text{lysogeny}}(M)$ predicted using Equations 19 and 20, the latter parametrized using $\mu_n = \langle\lambda(n)\rangle$ in LBMM and SM, are shown in Figure S7B (MOI^*, a, and $q_{\max}$ were kept constant). Given the same $q_{\max}$, the reduced probability of $P(\lambda \geq \text{MOI}^*)$ in SM results in a lower predicted $f_{\text{lysogeny}}(M)$ as compared to that in LBM.

Please cite this article in press as: Nguyen et al., Coinfecting phages impede each other's entry into the cell, Current Biology (2024), https://doi.org/10.1016/j.cub.2024.05.032

Stochastic model of phage entry kinetics

Setup of the model

The model is depicted in Figure 2B, and the variables used in the following derivations are listed in Table S5. For cells adsorbed by n phages, the model outputs, at time t, the probability distribution of the number of intracellular phage genomes, $P(\lambda|n,t)$. In addition, the model also predicts the probability distribution of the time of the i-th phage entry, $P(T_i|n)$.

Our model is governed by three parameters: The entry probability of each adsorbed phage at infinite time (η); the rate (or probability per unit time) of entry initiation by each phage (k); and the time between entry initiation and detection (τ). We note that to capture the experimental data, these three parameters were further parametrized as functions of n (Equations 8 and 9).

In the following derivations, the basic rules of probability were applied as described in Papoulis[95] and Arfken et al.[96] Symbolic integration was performed using Wolfram Mathematica, and the analytical solutions were confirmed using a simulation (section "simulating the stochastic model").

Model assumptions

For a cell adsorbed by n phages, we assumed that only $m \leq n$ phages are capable of entering the cell. Biologically, a phage may not be entry-capable because of faulty capsid assembly or DNA packaging, improper docking to the cell's receptors, ionic conditions not conducive for DNA ejection, or other reasons.[33,51,53,54,97,98] The probability per phage of being entry-capable is designated η. Thus, with n adsorbed phages on the cell, m follows a binomial distribution with a mean of ηn.

We assumed that each of the entry-capable phages has a probability of initiating entry per unit of time (i.e., a rate) equal to k. For a cell with m entry-capable phages, the probability per unit of time that an entry event is initiated by any of the phages is mk. The waiting time until the first entry initiation, $t_{0,1}$, thus follows an exponential distribution with a rate mk.

Following entry initiation, phage DNA is assumed to take a time τ to translocate into the cell and become labeled by the ParB-*parS* system. The time of the first phage entry, as measured, is thus $T_1 = t_{0,1} + \tau$.

After one phage has initiated entry, the number of remaining entry-capable phages is $m - 1$. The waiting time between the first and the second entry initiations, $t_{1,2}$, thus follows an exponential distribution with a rate $(m-1)k$. The time of the second phage entry is thus $T_2 = t_{0,1} + t_{1,2} + \tau$.

The same assumptions apply to the subsequent phages until all m entry-capable phages have entered the cell. Therefore, the time of the i-th phage entry is:

$$T_i = \tau + \sum_{j=1}^{i} t_{j-1,j}, \qquad \text{(Equation 21)}$$

where $t_{j-1,j}$ is the waiting time between the $(j-1)$-th and j-th entry initiations. Once all entries have occurred, the number of intracellular phage genomes is equal to the initial number of entry-capable phages, $\lim_{t\to\infty} \lambda(t) = m$.

Time-dependent average number of intracellular phage genomes

Following the assumptions above, an expression for the average number of intracellular phage genomes, $\langle\lambda(n,t)\rangle$, can be derived as follows. The rate of change in the average number of entry-capable phages that have not yet ejected their genomes ("unejected"), $\langle U(t)\rangle$, is given by:

$$\frac{d\langle U\rangle}{dt} = -k\cdot\langle U(t)\rangle. \qquad \text{(Equation 22)}$$

The solution of this ordinary differential equation, using the initial condition of $\langle U(t=0)\rangle = \langle m\rangle = \eta n$, is:

$$\langle U(n,t)\rangle = n\eta e^{-kt}. \qquad \text{(Equation 23)}$$

Accounting for the delay between entry initiation and detection (τ), the time-dependent average number of detected intracellular phage genomes in cells adsorbed by n phages is:

$$\langle\lambda(n,t)\rangle = \langle m\rangle - \langle U(t)\rangle = n\eta\left(1 - e^{-k(t-\tau)}\right) \text{ for } t \geq \tau, \text{and 0 otherwise.} \qquad \text{(Equation 24)}$$

Equation 24 was used to predict the average number of intracellular phage genomes in Figures 2C, 2E, 2H, S2D, S2F, and S2G.

The probability distribution of phage entry time, given m

With regard to the stochastic model, we first aimed to derive the probability density function (PDF) of the time of the i-th phage entry, given m entry-capable phages. Following Equation 21, this PDF was found using the convolution of the individual PDFs of the $t_{j-1,j}$ terms (each of which follows an exponential distribution with a rate equal to the product of k and the number of remaining entry-capable phages):

$$f(T_i = t|m) = f_{T_i|m}(t) = \binom{m}{i} ike^{-(m-(i-1))k(t-\tau)}\left(1 - e^{-k(t-\tau)}\right)^{i-1} \qquad \text{(Equation 25)}$$

for $t \geq \tau$ and $m \geq i$, and 0 otherwise.

Please cite this article in press as: Nguyen et al., Coinfecting phages impede each other's entry into the cell, Current Biology (2024), https://doi.org/10.1016/j.cub.2024.05.032

We used this PDF to derive the cumulative distribution function (CDF) of the time of the i-th phage entry, given m entry-capable phages:

$$F(T_i \leq t|m) = F_{T_i|m}(t) = \binom{m}{i} i(-1)^i \sum_{j=1}^{i} (-1)^j \binom{i-1}{j-1} \frac{1 - e^{-(m-(j-1))k(t-\tau)}}{m-(j-1)} \quad \text{(Equation 26)}$$

for $t \geq \tau$ and $m \geq i$, and 0 otherwise.

The first moment of the PDF $f_{T_i|m}(t)$ is the average time of the i-th phage entry, given m entry-capable phages:

$$\langle T_i(m) \rangle = \tau + \sum_{j=1}^{i} \frac{1}{(m-(j-1))k} \text{ for } m \geq i. \quad \text{(Equation 27)}$$

The probability distribution of phage entry time, given n

Equations 25, 26, and 27 above are conditional on the number of entry-capable phages, m. However, the observable in our experiments was not m, but the number of adsorbed phages, n. As m follows a binomial distribution with a "success" probability of η, given n adsorbed phages, the joint PDF for a cell to have m entry-capable phages and the i-th entry time to occur at $T_i = t$ is the product of the probability mass function (PMF) of m, $P(m|n)$, and $f_{T_i|m}(t)$ (Equation 25):

$$f(T_i = t, m|n) = f_{T_i,m|n}(t) = P(m|n) \times f_{T_i|m}(t)$$

$$= C^{-1} \binom{n}{m} \eta^m (1-\eta)^{n-m} \binom{m}{i} ike^{-(m-(i-1))k(t-\tau)} \left(1 - e^{-k(t-\tau)}\right)^{i-1} \quad \text{(Equation 28)}$$

for $t \geq \tau, m \geq i$, and $n \geq i$, and 0 otherwise,

in which $C = \sum_{j=i}^{n} \binom{n}{j} \eta^j (1-\eta)^{n-j}$ is a normalization constant. This renormalization was necessary because the supports of $P(m|n)$, defined for $m \in [0,n]$, and of $f_{T_i|m}(t)$, defined for $m \geq i$, are different.

The PDF of the time of the i-th phage entry, given n adsorbed phages (regardless of how many of which are entry-capable), was found by summing the joint PDF $f_{T_i,m|n}(t)$ in Equation 28 over all supported values of $m \in [i,n]$:

$$f(T_i = t|n) = f_{T_i|n}(t) = \sum_m f_{T_i,m|n}(t)$$

$$= C^{-1} \sum_{m=i}^{n} \binom{n}{m} \eta^m (1-\eta)^{n-m} \binom{m}{i} ike^{-(m-(i-1))k(t-\tau)} \left(1 - e^{-k(t-\tau)}\right)^{i-1} \quad \text{(Equation 29)}$$

for $t \geq \tau$ and $n \geq i$, and 0 otherwise.

Similarly, the average time of the i-th phage entry given n adsorbed phages was found using $P(m|n)$ and $\langle T_i(m) \rangle$ (Equation 27):

$$\langle T_i(n) \rangle = \sum_m P(m|n) \times \langle T_i(m) \rangle = \tau + C^{-1} \sum_{m=i}^{n} \left[\binom{n}{m} \eta^m (1-\eta)^{n-m} \sum_{j=1}^{i} \frac{1}{(m-(j-1))k} \right] \quad \text{(Equation 30)}$$

for $n \geq i$.

The probability distribution of the intracellular phage number at time t, given n

At time t, a cell would have exactly $\lambda = i$ intracellular phage genomes if the i-th phage entry has occurred by time t, but the $(i+1)$-th phage entry has not occurred yet. Therefore, given m entry-capable phages, the probability that a cell has $\lambda = i$ intracellular phage genomes at time t is:

$$P(\lambda = i|m,t) = F_{T_i|m}(t) - F_{T_{i+1}|m}(t), \quad \text{(Equation 31)}$$

in which $F_{T_i|m}(t)$, defined as the CDF of the entry time (Equation 26), describes the probability that the entry time of the i-th phage is less than or equal to t.

The joint probability for a cell to have m entry-capable phages and $\lambda = i$ intracellular phage genomes at time t, given n adsorbed phages, is the product of $P(m|n)$ and $P(\lambda = i|m,t)$ (Equation 30):

$$P(\lambda = i, m|n,t) = P(m|n) \times P(\lambda = i|m,t) = \binom{n}{m} \eta^m (1-\eta)^{n-m} \left(F_{T_i|m}(t) - F_{T_{i+1}|m}(t)\right). \quad \text{(Equation 32)}$$

Please cite this article in press as: Nguyen et al., Coinfecting phages impede each other's entry into the cell, Current Biology (2024), https://doi.org/10.1016/j.cub.2024.05.032

The probability that a cell has $\lambda = i$ intracellular phage genomes at time t, given n adsorbed phages, was found by summing the joint probability in Equation 32 over all values of $m \in [i, n]$ (recall that $F_{T_i|m}(t) = 0$ for $m < i$):

$$P(\lambda = i|n,t) = \sum_m P(\lambda = i, m|n,t) = \sum_{m=i}^{n} \binom{n}{m} \eta^m (1-\eta)^{n-m} \left(F_{T_i|m}(t) - F_{T_{i+1}|m}(t)\right). \quad \text{(Equation 33)}$$

Equation 33 was used to predict the theoretical distributions of intracellular phage numbers in Figures 2G and S2E.

Using Equation 33, we arrived at the expression for the average number of intracellular phage genomes at time t, given n adsorbed phages:

$$\langle \lambda(n,t) \rangle = \sum_{i=0}^{n} i \cdot P(\lambda = i|n,t) = \sum_{i=0}^{n} i \cdot \left[\sum_{m=i}^{n} \binom{n}{m} \eta^m (1-\eta)^{n-m} \left(F_{T_i|m}(t) - F_{T_{i+1}|m}(t)\right) \right]. \quad \text{(Equation 34)}$$

Substituting $F_{T_i|m}(t)$ from Equation 26 and integer values of $n \in [0, 20]$ into Equation 34, we recovered the same expression for $\langle \lambda(n,t) \rangle$ obtained from the mean-field model, Equation 24.

The case of cells with a single adsorbed phage

For convenience, some simple expressions for the case of $n = 1$ are written below. From Equation 29, the PDF of the phage entry time in cells adsorbed by one phage (shown in Figure 2D) is:

$$f(T_1 = t|n = 1) = k e^{-k(t-\tau)} \text{ for } t \geq \tau, \text{and 0 otherwise.} \quad \text{(Equation 35)}$$

From Equation 30, the average time of phage entry in cells adsorbed by one phage is:

$$\langle T_1(n = 1) \rangle = \tau + \frac{1}{k}. \quad \text{(Equation 36)}$$

In both Equations 35 and 36, because the entry time is only defined in cells with phage entry, the parameter η (controlling whether the adsorbed phage is entry-capable) does not appear in the expressions.

Because λ is either 0 or 1 for $n = 1$, the probability that a singly-adsorbed cell has one intracellular phage genome at time t (from Equations 26 and 33) and the time-dependent average number of intracellular phage genomes in singly-adsorbed cells (shown in Figure 2C) share the same expression:

$$P(\lambda = 1|n = 1,t) = \langle \lambda(n = 1,t) \rangle = \eta\left(1 - e^{-k(t-\tau)}\right) \text{ for } t \geq \tau, \text{and 0 otherwise.} \quad \text{(Equation 37)}$$

Simulating the stochastic model

Description of the simulation

This stochastic simulation was based on the mathematical model described above in section "stochastic model of phage entry kinetics" and utilized the Gillespie algorithm.[99] Below, we briefly summarize the pertinent parts of the model in the language of the simulation.

We assumed that an entry-capable phage exists in either one of the following two states: Adsorbed on the cell but unejected ("Outside"), or having ejected its DNA, now intracellular ("Inside"). There is only one forward reaction: A phage can transition from the "Outside" state to the "Inside" state using an "Ejection" reaction at a rate constant of k. For a cell with m entry-capable phages and $\lambda(t)$ "Inside" phages at time t, the time-dependent number of "Outside" phages is $m - \lambda(t)$. Hence, the propensity for the "Ejection" reaction is:

$$a_{\text{ejection}} = (m - \lambda)k. \quad \text{(Equation 38)}$$

Because there is no reverse reaction, eventually, all entry-capable phages will be "Inside", i.e., $\lim_{t \to \infty} \lambda(t) = m$. This serves as the terminal condition in the simulation.

Simulation algorithm

Prior to simulation, the MATLAB random number generator was seeded using 'rng('shuffle')'. For a cell adsorbed by n phages, with $t = 0$ defined as the time of phage adsorption:

(1) Determine the parameters (η, k, τ) that govern the dynamics of phage entry in this cell.

If these parameters are to be MOI-dependent, use the parametrization in Equations 8 and 9 above.

(2) Draw m, the number of entry-capable phages, randomly from a binomial distribution with parameters n and η (implemented using the MATLAB 'binornd' function).
(3) Initialize the system: $t = 0$ and $\lambda(t = 0) = 0$.
(4) Simulate the waiting time between phage entries:
  (4.1) Calculate the ejection propensity (using Equation 38).
  (4.2) Draw a random number r from a uniform distribution in the unit interval (implemented using the MATLAB 'rand' function).

Please cite this article in press as: Nguyen et al., Coinfecting phages impede each other's entry into the cell, Current Biology (2024), https://doi.org/10.1016/j.cub.2024.05.032

(4.3) Calculate the waiting time until the next entry initiation:

$$t_{\text{waiting}} = \frac{1}{a_{\text{ejection}}} \log \frac{1}{1-r}. \quad \text{(Equation 39)}$$

(4.4) Record t_{waiting} into a vector of waiting times between entry initiations, $\mathbf{t}_{\text{between}}$.
(4.5) Update the system: $t \leftarrow t + t_{waiting}$, and $\lambda \leftarrow \lambda + 1$.
(4.6) If $\lambda = m$, terminate the waiting-time simulation and proceed to step 5. Else, return to step 4.1.
(5) Determine the time from adsorption to the initiation of each phage entry, $\mathbf{t}_{\text{initiation}}$, equal to the cumulative sum of $\mathbf{t}_{\text{between}}$.
(6) Determine the time from adsorption to when the intracellular phage genome is detected, $\mathbf{t}_{\text{entry}} = \mathbf{t}_{\text{initiation}} + \tau$. This is equivalent to the phage entry times as experimentally measured.

Processing of simulation results

The simulation was performed for $n \in [0,20]$, with 10000 cells for each n value. For each simulated cell, the vector of simulated entry times was processed as a series of entry events following synchronized adsorptions. We confirmed that the observables produced by this stochastic simulation are in agreement with the analytical solution described in section "stochastic model of phage entry kinetics".

Stochastic simulation of infection outcome in individual cells

Summary of the mathematical model in Yao et al.

Our simulation for the infection outcome was based on the model in Yao et al.[8] Below, we briefly describe this model where pertinent to the current work.

Yao et al. modeled the cell-fate decision of phage lambda using a set of ordinary differential equations (ODEs) that track the mRNA and protein concentrations of three genes governing the decision: *cI*, *cII*, and *cro*, as well as the concentration of the phage genomes in the infected cell. The cell volume was assumed to grow exponentially over time. The input of the model is the initial viral concentration, defined to be the MOI divided by the initial cell volume. The MOI is the initial intracellular number of phage genomes; the model in Yao et al. was agnostic to the number of adsorbed phages or the phage-to-bacteria ratio in the environment. The initial cell volume was set to be 1 μm^3, uniform for all cells. Depending on whether infection of a replication-competent or replication-deficient phage is modeled, the copy number of the phage genomes may increase over time. The ODEs were solved numerically to yield the kinetics of Cro (driving lysis) and CI (driving lysogeny), whose concentrations were compared to respective thresholds to determine the cell fate. Four outcomes are possible: Failed infection, lysis, lysogeny, and mixed outcome (Figure S7C).

Because the initial cell volume is assumed uniform, the predicted cell fate for a given MOI is deterministic, and the frequency of lysogeny is a step-function of MOI. In particular, for infection by replication-competent phages, cells with MOI = 1 are lytic, while cells with MOI $\geq$ 2 are lysogenic.

Summary of the single-cell data in Zeng et al.

We aimed to compare our simulation results with the single-cell data from Zeng et al.[6] Below, we briefly describe this data where pertinent to this study.

Zeng et al. measured the fate of individual cells following infection by a replication-competent phage strain. Capsids of the infecting phages were fluorescently labeled using a scheme similar to the current study, and the single-cell MOI was defined as the number of phages adsorbed to the cell (Zeng et al. did not measure the number of intracellular phage genomes). After 30 minutes of incubation at low temperature to allow phages to adsorb to the cell and 5 minutes at 35°C to trigger phage ejection, the infection mixtures in Zeng et al. were diluted using room-temperature (RT) medium, mounted, and imaged in a time-lapse at RT. The infected cells harbored fluorescence reporters that enabled the detection of cell fate. In Zeng et al., the measured frequency of lysogeny increased gradually with the number of adsorbed phages.

In addition, Zeng et al. found cell size to affect the infection outcome. For a given MOI, smaller cells had a higher chance of being lysogenized. The distribution of normalized cell size in Zeng et al. was approximated as a log-normal distribution ($\mu = 1, \sigma = 0.28$).

Description of our simulation

We performed the following simulation for cells adsorbed by $n \in [0,5]$ phages, with 1000 cells for each n value.

For a cell adsorbed by n phages:

(1) Determine the initial cell size (drawn from a log-normal distribution, described in below).
(2) Determine the single-cell MOI (accounting for stochastic phage entries, described in below).
(3) Calculate the initial viral concentration.
(4) Apply the Yao et al. model to determine the cell fate.

The system of ODEs from Yao et al. was solved for infection by replication-competent phages as described in the original paper. The frequency of lysogeny was calculated as the fraction of lysogenic cells among lytic or lysogenic cells (i.e., failed infection and

Please cite this article in press as: Nguyen et al., Coinfecting phages impede each other's entry into the cell, Current Biology (2024), https://doi.org/10.1016/j.cub.2024.05.032

mixed outcome were not included). Following how Zeng et al. reported the data, the decision curve (Figure 6B) depicts the frequency of lysogeny as a function of the number of adsorbed phages, $f_{\text{lysogeny}}(n)$, regardless of how many intracellular phage genomes are in the cell.

Incorporating variations in cell size

We first aimed to introduce variations in cell size into the Yao et al. model. For each cell with a given number of adsorbed phages (n), we randomly generated the initial cell size by drawing from a log-normal distribution with $\mu = 1, \sigma = 0.28$ (as described in Zeng et al.), implemented using the MATLAB 'lognrnd' function. This initial cell size was used to calculate the initial viral concentration, with the MOI equal to the number of adsorbed phages.

Variations in cell size introduced some variability to the cell fate. In particular, while Yao et al. deemed all cells with MOI = 1 to be Cro-dominant, thus lytic, variations in cell size rendered approx. 20% of the cells lysogenic. This fraction reflected infection in very small cells, such that the initial concentration of phage genomes was higher, facilitating increased CI concentration (Figure S7C), thus lysogeny. Because infection in very large cells reduced the initial viral concentration, for MOI = 2, the frequency of lysogeny decreased from 100% in Yao et al. to approx. 98%. Variations in cell size did not change the frequency of lysogeny for MOI higher than 2. We used these predictions by the model with cell size variations as a baseline to determine the effect of phage entry dynamics on the infection outcome.

Incorporating stochastic phage entry

Next, we introduced stochastic phage entries into the model with cell size variation. For each cell with a given number of adsorbed phages (n), we implemented the simulation of stochastic phage entries (described in section "simulating the stochastic model") to determine the time series of phage entries in this cell. On average, the simulated number of intracellular phage genomes was lower than the number of adsorbed phages, and the phage genomes entered the cell non-simultaneously. Because Zeng et al. diluted the infection mixture using RT medium and imaged the cells at RT, effectively halting additional phage entries after 5 minutes, we set the MOI that drives the lysis vs. lysogeny decision to be the number of phage genomes that have entered the cell within 5 minutes. The initial viral concentration is thus $\lambda(t = 5\ \text{min})$ divided by the initial cell size (drawn from a log-normal distribution as above).

Stochastic phage entries had a strong effect on the decision curve (Figure 6B). For example, among cells adsorbed by $n = 2$ phages, approx. 50% of the cells had only one intracellular phage genome by 5 minutes. In such cells, the increased concentration of Cro (Figures 6A and S7C) rendered the cell lytic. Similarly, the frequency of lysogeny also decreased for MOI higher than 2, and even in cells adsorbed by 5 phages, not all of the infected cells were lysogenic (Figure S7D).

We note that within our simulation framework, stochastic phage entries had no effect on the infection outcome of MOI = 1. For this MOI, failed or delayed phage entry, which would result in failed infection (Figure S7D), did not change the decision curve, which was calculated based on the ratio between the lytic and lysogenic cells only.

Fitting to the Hill function

The Hill equation (below) was fitted to the frequency of lysogeny as a function of the number of adsorbed phages, $f_{\text{lysogeny}}(n)$, for the data from Zeng et al. and our simulation results.

$$f_{\text{lysogeny}}(n) = \frac{n^h}{K^h + n^h}. \quad \text{(Equation 40)}$$

In Equation 40, h is the Hill coefficient, which describes the degree of precision in the decision curve,[70] and K is the MOI at which the frequency of lysogeny reaches half its maximum. For Zeng et al., data for "all cells" in Figure 2C of the original paper was extracted, and bootstrapping was performed by resampling the mean values. For our simulation results, bootstrapping was performed on the single-cell level as described above.

Fitting results are shown in Figure 6B. The simulation with cell size variation alone gave $h = 7.87 \pm 0.41$, $K = 1.18 \pm 0.01$. The simulation with both cell size variation and stochastic phage entries gave $h = 1.84 \pm 0.08$, $K = 1.81 \pm 0.05$. Refitting Zeng et al. data gave $h = 0.94 \pm 0.20$, $K = 1.71 \pm 0.29$, similar to the published values, $h = 1.0 \pm 0.1$, $K = 1.8 \pm 0.1$.

QUANTIFICATION AND STATISTICAL ANALYSIS

Data analysis and modeling were performed using MATLAB as described above. The statistical details of each experiment, including sample size, calculation of error bars or uncertainty values, and p-values where appropriate, are provided in the legends and captions of the graphs, or in the corresponding STAR Methods sections.